SYLVANIA ELECTRONIC SYSTEMS
WESTERN DIVISION

FREQUENCY STABILIZED GAS LASER

FINAL REPORT

Contract NAS 8-20631

1 October 1969

Prepared For

National Aeronautics
and
Space Administration
Huntsville, Alabama

SYLVANIA
GENERAL TELEPHONE & ELECTRONICS

SYLVANIA ELECTRONIC SYSTEMS - WESTERN DIVISION
Post Office Box 188
Mountain View, California 94040

FREQUENCY STABILIZED GAS LASER

FINAL REPORT

Contract NAS 8-20631

1 October 1969

M. W. Sasnett

APPROVED BY:

R. S. Reynolds, Head
Gas Laser Section
Electro-Optics Organization

D. E. Caddes, Manager
Research and Development Department
Electro-Optics Organization

Prepared For

National Aeronautics and Space Administration
Huntsville, Alabama

FOREWORD

This report is the final technical report documenting work performed in developing and testing a stabilized CO_2 laser communication system for NASA - Marshall Space Flight Center, Huntsville, Alabama. The work was performed under Contract NAS 8-20631 entitled "Stabilized CO_2 Lasers". This report was prepared by the Electro-Optics Organization of Sylvania Electronic Systems - Western Division, Mountain View, California, and describes work performed in the Research and Development Department, headed by Dr. Donald E. Caddes. Mr. Michael W. Sasnett was the principal technical participant during the final phase of the program. Other contributors during the program were Mr. R. S. Reynolds and Professor A. E. Siegman.

The work performed under this contract was administered by the Astrionics Laboratory of the NASA, Marshall Space Flight Center, Huntsville, Alabama. Dr. J. L. Randall and Mr. P. J. Marrero were the principal technical representatives for the Astrionics Laboratory.

ABSTRACT

This report presents details of the design, construction and test of a stabilized CO_2 laser heterodyne communication system operating at 10.59 microns. Calculations show that the expected heterodyne signal-to-noise ratio for a 4 km atmospheric path is approximately 63 dB. Two-megahertz-bandwidth phase modulation of the 1-watt transmitter laser with a modulation depth of 0.22 is provided by an electro-optic GaAs phase modulator. Transmitting and receiving antennae are 4 1/4 inch diameter f/4.5 Newtonian telescopes. Local oscillator and signal beams are mixed on a Ge:Au detector to provide a 10 MHz i.f. which is maintained by an AFC loop which keeps the local oscillator laser's frequency offset from the transmitter laser by 10 MHz. Spectrum analysis of the unmodulated i.f. signal shows a characteristic linewidth of about 6 kHz with slow drifting of the i.f. within ±20 kHz. Detection of the phase information after amplification of the i.f. is by means of an FM discriminator followed by a broadband integrator. Measurements of system performance over a short indoor propagation path showed a large noise component at low frequencies, due to phase instability between laser oscillators. This noise was suppressed by limiting of system response at low audio frequencies. Suppression of modulator resonances is discussed. A method for relatively easy conversion of the system to AM transmission is described. Such a conversion will allow comparative evaluation of the two types of systems.

TABLE OF CONTENTS

Section	Title	Page
1.0	INTRODUCTION	1
2.0	10.6 MICRON COMMUNICATION SYSTEM	3
	2.1 Introduction	3
	2.2 System Description	4
	2.3 System Performance	10
3.0	COMPONENTS FOR COMMUNICATION SYSTEM	17
	3.1 Introduction	17
	3.2 CO_2 Laser	17
	3.2.1 CO_2 Laser Operating Characteristics	17
	3.2.2 Laser Design	21
	3.2.3 Mechanical Design	22
	3.2.4 Plasma Tube Design	30
	3.3 GaAs Phase Modulator	31
	3.4 Modulator Driver	36
	3.5 Telescope	40
	3.6 Receiver Electronics	40
	3.6.1 Introduction	40
	3.6.2 Detector	40
	3.6.3 I.F. Amplifier and F.M. Limiter-Discriminator	43
	3.6.4 Integrator	46
	3.6.5 AFC Circuit	49
	3.7 Transmitter System	52
	3.8 Receiver System	57
4.0	SYSTEM PERFORMANCE	62
	4.1 Introduction	62
	4.2 Optical Power Flow	62
	4.3 Receiver Electronics Performance	63
5.0	CONCLUSIONS AND RECOMMENDATIONS	70
6.0	REFERENCES	72

LIST OF ILLUSTRATIONS

Figure	Title	Page
2-1	Block Diagram of CO_2 Laser Transmitter.	6
2-2	Layout of CO_2 Laser Transmitter.	7
2-3	Block Diagram of CO_2 Laser Receiver.	8
2-4	Layout of CO_2 Laser Receiver.	9
2-5	Power Flow in Receiver.	13
3-1	Relationship of Cavity Resonances to P(J) Gain Lines.	20
3-2	Laser Cavity Assembly.	25
3-3	Stable 0.5 Meter CO_2 Laser.	27
3-4	Schematic of CO_2 Laser Temperature Controller.	28
3-5	Laser Cavity Temperature Controller.	29
3-6	GaAs Electro-Optic Modulator.	34
3-7(a)	Phase Modulation Sidebands Before Clamping Modulator Rods in Lead.	35
3-7(b)	Phase Modulation Sidebands After Calmping Modulator Rods in Lead.	35
3-8	Schematic Diagram of Broadband Modulator Driver.	37
3-9	Modulator Driver Frequency Response.	38
3-10	Phase Modulator Driver.	39
3-11	Block Diagram of Receiver.	41
3-12	Photograph of Laser Receiver Electronics.	42
3-13	Schematic Diagram of Detector Bias and Interlock Circuit.	44
3-14	Schematic Diagram of I.F. Amplifier.	47
3-15	Schematic Diagram of Limiter-Discriminator.	48
3-16	Schematic Diagram of Integrator Circuit.	50
3-17	Schematic Diagram of AFC Amplifier Circuit.	51
3-18	Photograph of 10.6 Micron Transmitter.	53
3-19	Transmitter Control Console.	54
3-20	Transmitter Electrical Interconnection Diagram.	56
3-21	Photograph of 10.6 Micron Receiver.	58
3-22	Receiver Control Console.	59

LIST OF ILLUSTRATIONS

Figure	Title	Page
3-23	Receiver Electrical Interconnection Diagram.	60
3-24	10.6 Micron Communication System.	61
4-1	Heterodyne Beat Frequency Before and After Activation of AFC.	64
4-2	Spectrum Analyzer Display of Heterodyne Beat Signal for Two Different Observation Periods.	66
4-3	Spectrum Analysis of Receiver Low Frequency Noise Output.	67
4-4	Receiver Output Amplitude vs. Frequency for 0.5 V (peak) Signal Input at Transmitter.	68

LIST OF TABLES

Table	Title	Page
3-1.	Lowest Longitudinal Mode Frequencies in Invar Laser Cavities	23
3-2	Detector Specifications	43
3-3	I.F. Amplifier Seecifications	45
3-4	FM Limiter-Discriminator Specifications	45
3-5	D.C. Gain of Elements in AFC Loop	52
3-6	Plasma Power Supply Specifications	55
4-1	Optical Power Levels in Transmitter at 10.59 Microns	62
4-2	Optical Power Levels in Receiver at 10.59 Microns	63

SECTION 1.0
INTRODUCTION

As a signal source for optical communications, radar and interferometry, the carbon dioxide laser has important advantages over other laser oscillators: It is presently capable of higher efficiency than any other laser and the 10.6 micron output wavelength falls within an excellent band for propagation through the atmosphere.

These potentials for the CO_2 laser were recognized early during its development period and a program was undertaken to develop two frequency-stabilized lasers for use in optical heterodyne experiments. The method chosen to accomplish long-term absolute frequency stabilization of the laser involved locking it to the center of one of the CO_2 transition frequencies near 10.6 microns.[1-1, 2] This reference line was to be sensed in a CO_2 amplifier tube, separate from the laser oscillator. The scheme involved phase-modulating a fraction of the laser output and then detecting the frequency sensitive distortion of this modulation produced by the CO_2 amplifier. The distortion was expected to produce an error signal which could be used to stabilize the laser frequency.

Experiments were carried out to determine the feasibility of this technique. Results showed that the discriminant obtained in this way was an order of magnitude less sensitivie than had been expected. This was due to a large homogeneous broadening of the amplifier linewidth when the amplifier gain was optimized resulting in the flattening of the CO_2 gain profile. Measurements of the gain profile under varying operating conditions and the resulting effect on the degree of stabilization are described in another contract report.[1-3]

Because of this effect, we could predict frequency stability of only a part in 10^{-8} or 10^{-9}. The program was therefore redirected to the effort reported here: The equipment which had been developed for the stabilized lasers was utilized in the construction of a one-way heterodyne communication system using broadband phase modulation. The components

made available from the previous work included the following:

1. Two 1-watt single-frequency CO_2 lasers with short-term frequency stability (RF spectrum width) of a few parts in 10^{10} and long-term stability of about ±2 parts in 10^7 (±6 MHz) over several hours.
2. GaAs optical phase modulators capable of 0.5 radian peak phase modulation depth per kilovolt.
3. Ge:Au 10.6 micron detectors and associated bias electronics.
4. Power supply consoles for two laser systems.

This report describes the design and construction of a system using these components and presents the results of limited testing performed with the system. Section 2 presents both a description of the system and calculations which yield the expected heterodyne signal-to-noise performance for an atmospheric propagation path of 4 kilometers. Section 3 describes the components used in the system in detail, and Section 4 presents the results of performance tests made over a short indoor path. Conclusions and recommendations are given in Section 5, and Section 6 lists the references used in the text.

SECTION 2.0

10.6 MICRON COMMUNICATION SYSTEM

2.1 Introduction

The carbon dioxide laser is a very attractive source for use in communication systems due to its high efficiency and because its emission wavelengths are in a spectral region where the earth's atmosphere is exceptionally transparent. At the wavelengths near 10.6 microns, effects including phase front distortion, scattering and absorption in the atmosphere are very much reduced in magnitude from the effects observed at shorter visible wavelengths. The 10.6 micron wavelengths are still sufficiently short that aperture (antenna) dimensions can be very small relative to those required at radio and microwave frequencies. The narrow beam divergence and narrow receiver field of view make wideband communications with minimum interference an attractive feature of 10.6 micron communication systems just as with visible wavelength systems.

Modulators making use of the electro-optic effect in materials which are useful at 10.6 microns are much less effective than their counterparts at the visible wavelengths for essentially two reasons:

1) Known electro-optic materials which transmit well at 10.6 microns have relatively small electro-optic coefficients.
2) A given interaction length in terms of the number of optical waves involved is much longer at 10.6 microns than in the visible region requiring larger crystal length.

Kaminow has shown that for an electro-optic modulator in which the modulator crystal itself is the dominant capacitive impedance that, for a given bandwidth and modulation depth the power required will be proportional to (λ^3/F) where F is a figure of merit for the particular material involving index of refraction, electro-optic coefficient and low frequency dielectric constant.[2-1] The best electro-optic materials for 10.6 microns and in the visible region have very similar values for F (though its component values are quite different). The λ^3 dependence

of power is, therefore, not compensated for by the material properties and the approximately 20 times longer wavelength results in tremendously larger power requirements for the same information capacity at 10.6 microns.

Photon detectors for 10.6 micron radiation are also less effective than their counterparts at visible wavelengths, principally because there is no method as yet for making photoemissive surfaces for 10.6 microns. Whereas direct detection of weak visible signals becomes practical with a photoemitter followed by a relatively noise free electron multiplier, 10.6 micron detectors must use heterodyne multiplication of weak signals in order to overcome thermal and background noise. Also, 10.6 micron detectors must be cooled to very low temperatures in order that thermal generation of carriers in the detector material is not the dominant carrier generation process. This cooling entails added system complexity.

Because the disadvantages are offset by the advantages listed above, communications systems using the CO_2 laser are competitive with other types of systems, including both R.F. and visible types. Their greatest usefulness (as with other laser systems) will most probably be in space communications, although specialized terrestrial systems are also contemplated. Many experiments are currently under way to determine areas of greatest potential.

2.2 System Description

A laser heterodyne communication system has been constructed which provides a one-way 2-MHz-bandwidth communication channel at a 10.6 micron carrier wavelength. The system is designed for use in ground-to-ground applications; however, with the addition of acquisition and tracking capability there exists the possibility of air-to-ground or ground-to-air communication. This is made possible by the relatively compact and rugged nature of the transmitter and receiver units, and because the laser tubes are sealed-off and require no external pump or gas supply.

The transmitter for this system uses as its carrier source a sealed-off 1 watt CO_2 laser which has been designed to provide stable single-frequency oscillation on a single, selectable wavelength near 10.6 microns. Stable operation at that wavelength is maintained by close temperature control of the invar-aluminum laser cavity.

Phase modulation of the transmitted beam is provided by a GaAs electro-optic modulator which is external to the transmitter oscillator. The combined modulator and driving circuit provides 0.22 radians peak phase deviation for approximately 0.5 volt input signal. Frequency response is from 2 kHz to 2 MHz. The transmitting and receiving apertures (antennae) are identical and consist of 11 cm diameter Newtonian-type telescopes.

Figure 2-1 is a block diagram of the transmitter system and Figure 2-2 shows a diagram of the physical layout.

At the receiver, the local oscillator and received beams are combined on a NaCl beamsplitter and then focused onto a Ge:Au detector. Following the detector is an i.f. preamplifier and a frequency discriminator both operating at 10 MHz. A low-frequency output from the discriminator is used in an AFC circuit to maintain the local oscillator frequency at the 10 MHz offset from the transmitter laser. A video bandwidth output from the discriminator delivers a signal, corresponding to the instantaneous intermediate frequency, to a broadband integrating circuit which converts the FM analog back to an analog of the transmitted PM signal.

Figures 2-3 and 2-4 show the block diagram and physical layout for the receiver system.

Power and control functions for the transmitter and receiver are supplied by separate control consoles. The laser oscillators each require a regulated high voltage d.c. power supply which is in the console, and is interlocked to prevent operation of the lasers when cooling water is not

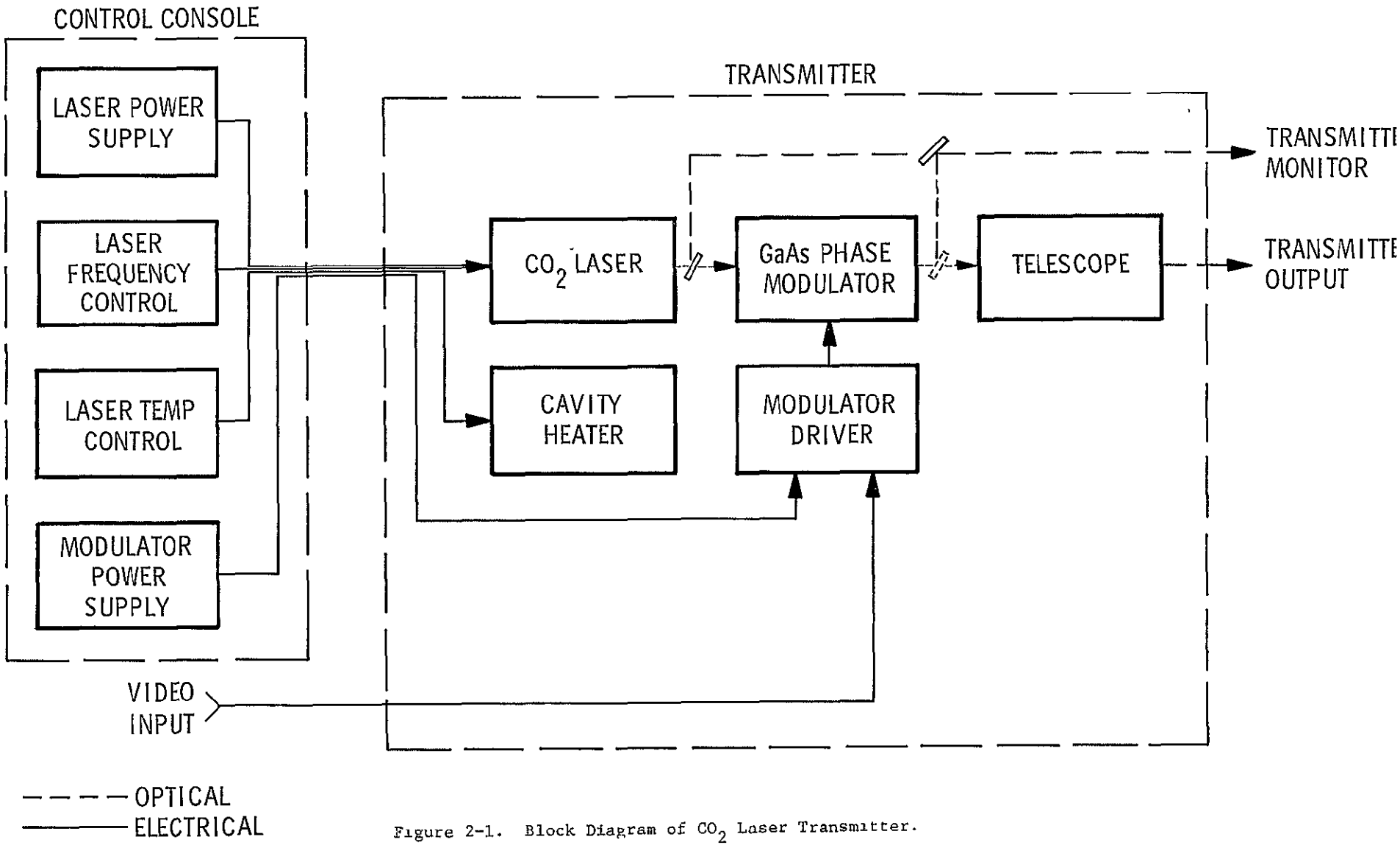

Figure 2-1. Block Diagram of CO_2 Laser Transmitter.

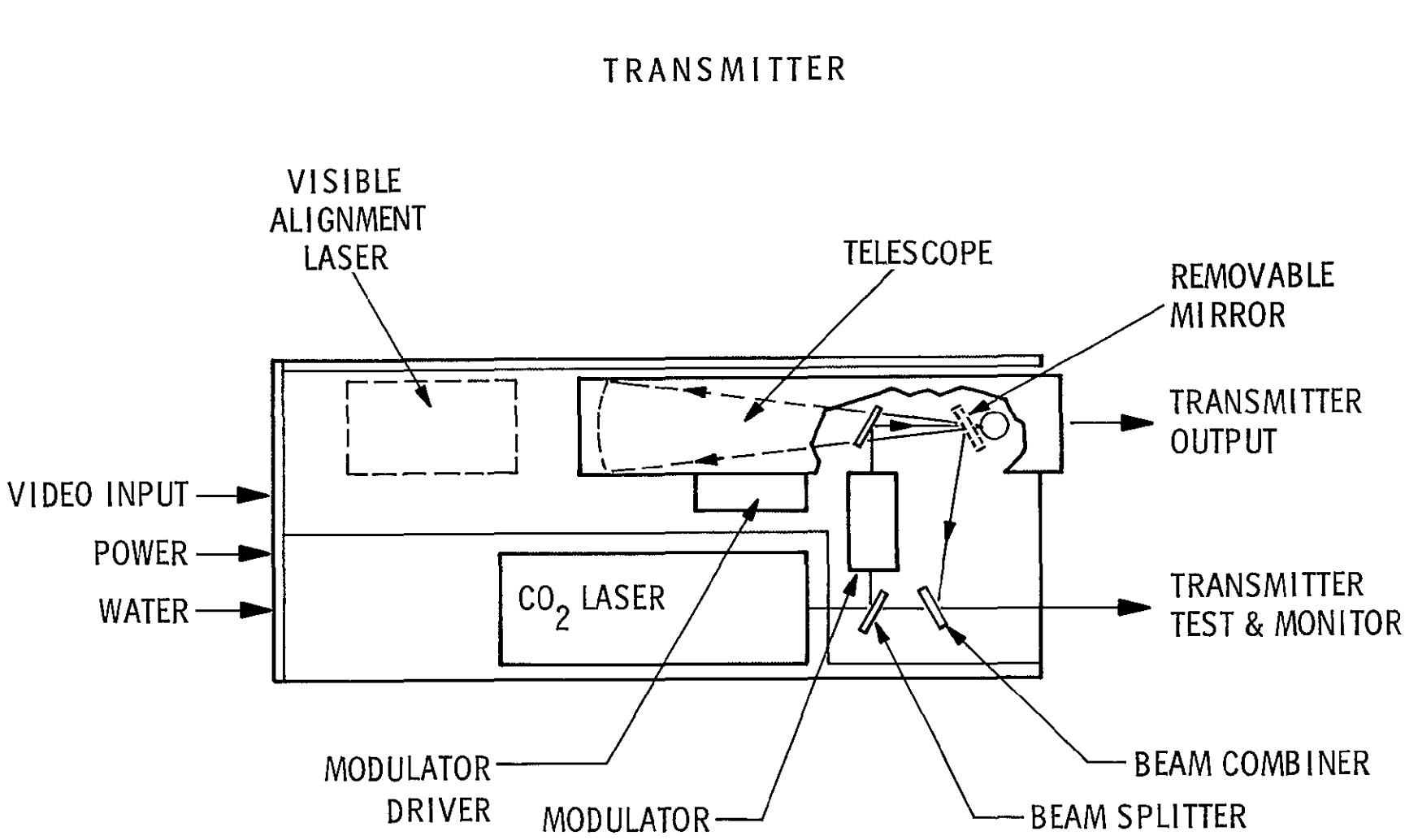

Figure 2-2. Layout of CO_2 Laser Transmitter.

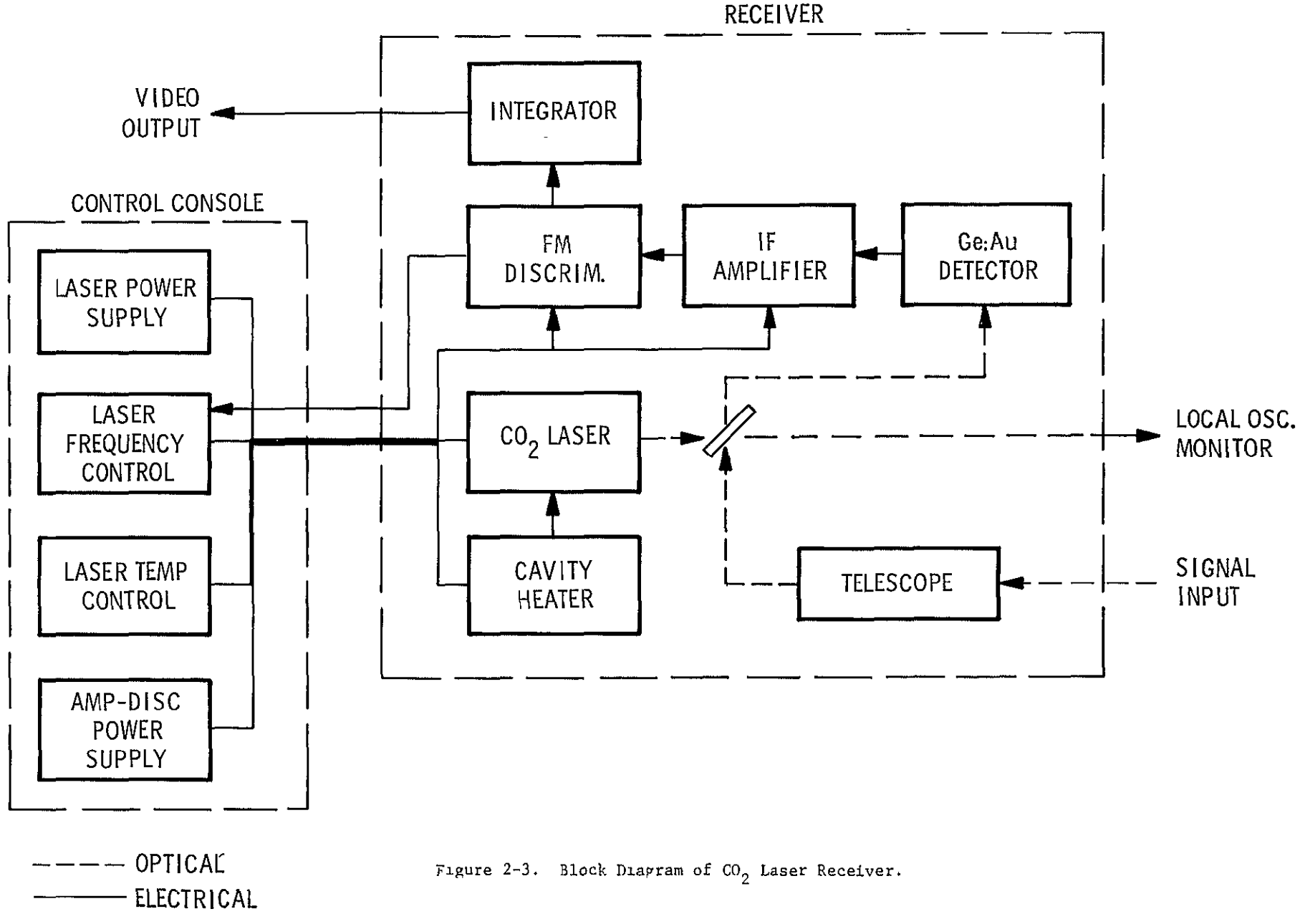

Figure 2-3. Block Diagram of CO_2 Laser Receiver.

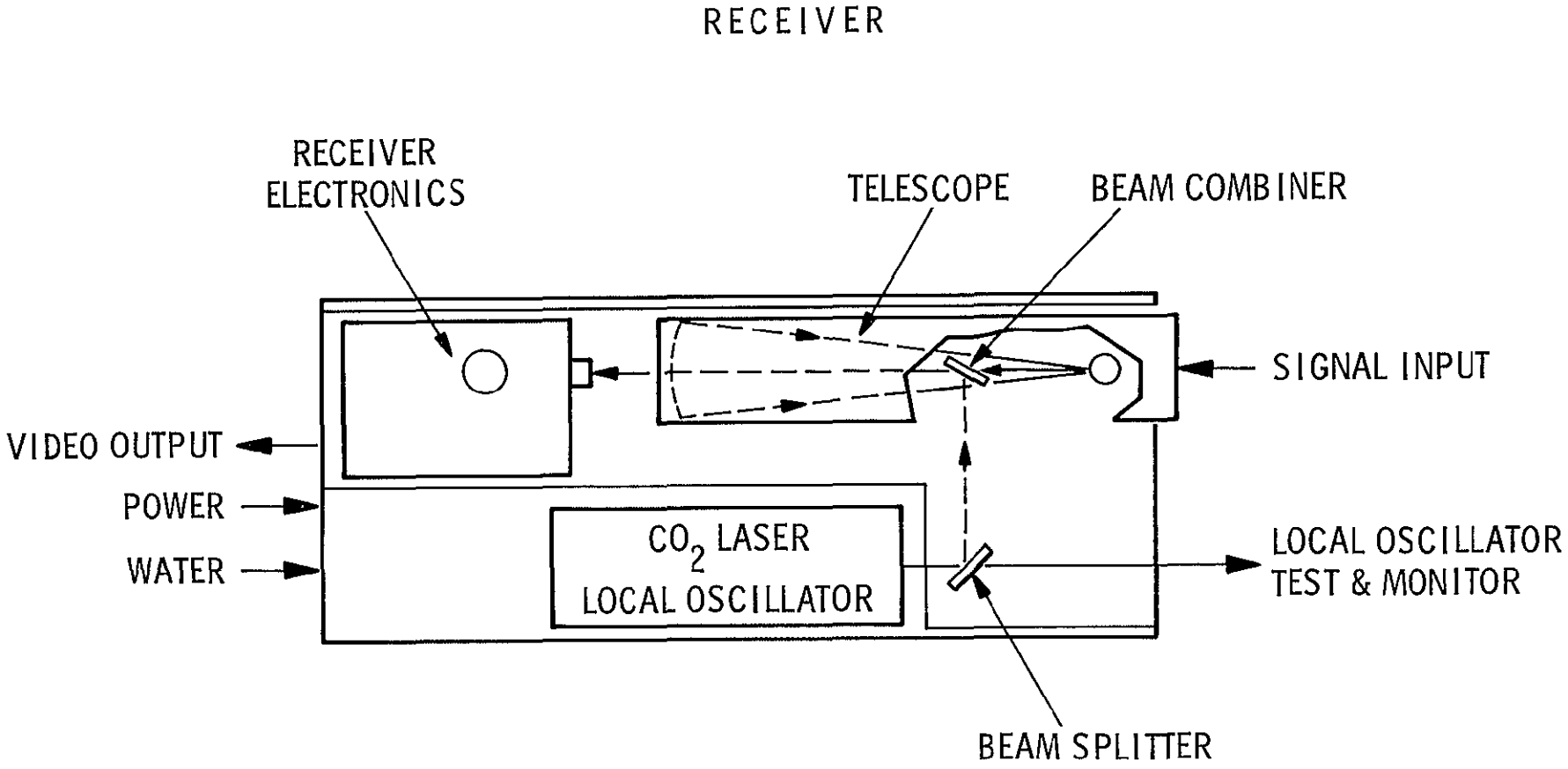

Figure 2-4. Layout of CO_2 Laser Receiver.

flowing. Both control consoles also house temperature control units for the lasers, and power supplies for the piezoelectric cavity tuners.

2.3 System Performance

For an optical receiver using heterodyne detection, the signal to noise ratio at the input terminals of the first amplifier in terms of the mean square currents involved can be written as

$$\frac{S}{N} = \frac{\left(\frac{e\eta G}{hf}\right)^2 2 P_{LO} P_S}{4 \frac{e^2 \eta G^2 B}{hf} (P_{LO} + P_S + P_B) + 4 kB \left(\frac{T_D}{R_D} + \frac{T_L}{R_L}\right)} \qquad (2\text{-}1)$$

where e is the charge on an electron, η is the quantum efficiency, G is the photoconductive gain of the detector, f is the optical frequency and B is the electrical bandwidth. P_{LO}, P_S and P_B are respectively the local oscillator, carrier signal and background power levels at the detector. T_D, T_L, R_D, R_L are the temperatures and resistances of the detector and load. Noise due to fluctuations in the frequency and amplitude of the carrier and local oscillator sources if not considered here.

To present system uses a gold-doped germanium photoconductor detector. The quantum efficiency of the Ge:Au detector is on the order of 0.04% at 10.6 microns and the photoconductive gain is about 0.2.[2-2] Using these figures in evaluating the generation-recombination noise term in equation 2-1 gives (per watt and per unit bandwidth),

$$\frac{\overline{i^2}_{G\text{-}R}}{PB} = \frac{4e^2 \eta G^2}{hf} = 8.8 \times 10^{-23} \frac{\text{amps}^2}{\text{watt - Hz}} \qquad (2\text{-}2)$$

The thermal noise term is evaluated using $R_D = 160\Omega k$, $T_D = 77^\circ K$, $R_L = 50\Omega$, and $R_L = 300^\circ K$. (It will be noted that the detector thermal noise is insignificant compared to the noise in the load resistance.)

$$\frac{\overline{i^2_{th}}}{B} = 4k\left[\frac{T_D}{R_D} + \frac{T_L}{R_L}\right] \cong \frac{4k\,T_L}{R_L} = 33 \times 10^{-23} \ \frac{\text{amps}^2}{\text{Hz}} \qquad (2\text{-}3)$$

Comparing (2-2) and (2-3), it will be seen that unless the total power on the detector is more than about 4 watts, thermal noise in the source resistance of the first amplifier will be the predominant noise source. With other detectors such as Ge:Cu and Hg-Cd-Te, the G-R noise term will predominate due to their higher quantum efficiencies allowing the heterodyne signal-to-noise ratio to approach the quantum noise limit.

In the present system (considering first no separation between the transmitter and receiver and hence no long-distance propagation losses) the sum of P_S and P_{LO} can never be more than about 1 watt, with a maximum of 0.6 watts available from the local oscillator. At typical operating ranges, the signal power will become insignificant compared to the local oscillator power and the signal-to-noise ratio can be written approximately

$$\frac{S}{N} = \frac{\left(\frac{enG}{hf}\right)^2 2\,P_{LO}\,P_S}{\frac{4\,kT_L\,B}{R_L}} \qquad (2\text{-}4)$$

The receiver performance will therefore be maximized by maximizing the product of P_{LO} and P_S.

At the beamsplitter which combines the local oscillator and signal beams, the power flow from these sources to the detector can be expressed in terms of the transmission of the beamsplitter, t, as

$$P_S = t\,P_{SA}$$
$$\text{and} \quad P_{LO} = (1-t)P_{LOA} \qquad (2\text{-}5)$$

where P_{SA} and P_{LOA} are respectively the available signal and local oscillator powers incident on the beamsplitter as shown in Figure 2-5. The product of P_S and P_{LO} may then be written as,

$$P_{LO}\, P_S = (t-t^2)P_{LOA}\, P_{SA} \tag{2-6}$$

Differentiation of (2-6) yields the condition for maximization of $P_{LO}\, P_S$, namely that;

$$t = 1/2 \tag{2-7}$$

Consequently, a 50% beamsplitter will be optimum for the system.

The expected (available) signal power at the receiver for a range of 4 kilometers is calculated as follows:

$$P_{SA}' = \frac{dP_t}{dA} A_r T \tag{2-8}$$

where dP_t/dA is the power per unit area which can be considered constant over the receiver aperture A_r, and T contains all the transmission efficiency factors.

The far field radiation pattern for a Gaussian beam which is closely approximated by a CO_2 laser in TEM_{oo} mode can be shown to be

$$\frac{dP_t}{dA} = \frac{2P_t}{\pi w^2} \exp\frac{-2r^2}{w^2} \tag{2-9}$$

where P_t is the power at the output of the transmitter telescope, $w = R\lambda/\pi a$ is the radius of the beam at which the intensity has dropped to $1/e^2$, and R, λ, and a are the range, wavelength, and the radius of the beam at the transmitter.

Substituting Equation (2-9) into Equation (2-8) for $r << w$ gives

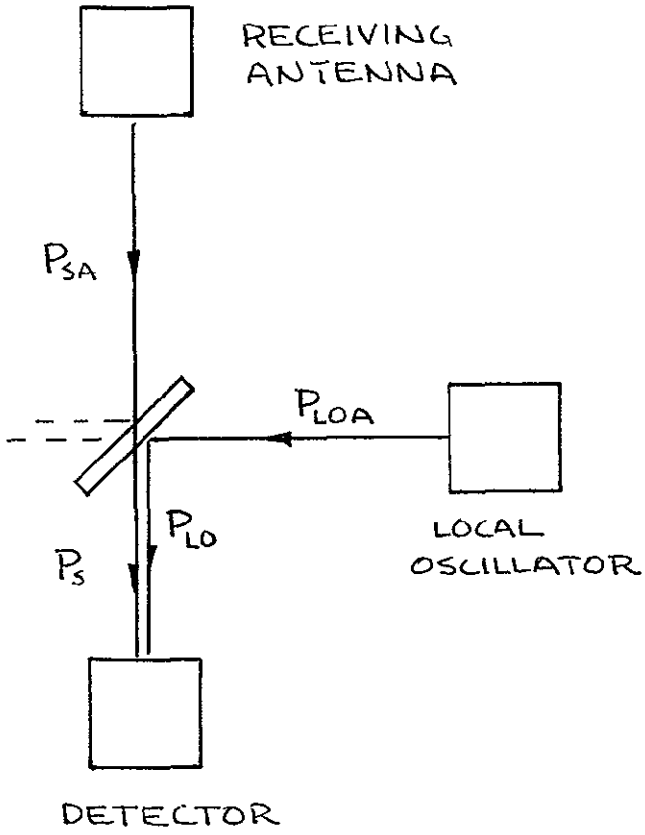

Figure 2-5 Power Flow in Receiver.

$$P_{SA} = \frac{2P_t}{\pi w^2} A_r T \qquad (2\text{-}10)$$

In terms of the transmitter optical antenna radius (a) and the antenna area $A_t = \pi a^2$

$$P_{SA} = \frac{2P_t A_r A_t T}{R^2 \lambda^2} \qquad (2\text{-}11)$$

Neglecting the value of T for the moment, and using the following values,

$P_t = 0.4$ watts (see section 3)

$A_r = A_t = 91.5$ cm^2 (4 1/2-inch diameter)

$R = 4 \times 10^5$ cm ($\sim$ 2.5 miles)

$\lambda = 10.6 \times 10^{-4}$ cm

we obtain,

$$\frac{P_{SA}}{T} = 37 \times 10^{-3} \text{ watts} \qquad (2\text{-}12)$$

and,

$$\frac{P_S}{T} = 18.5 \times 10^{-3} \text{ watts} \qquad (2\text{-}13)$$

For evaluation of the signal to noise ratio given by equation (2-4), the following quantities appropriate to the present system are used.

$\eta = 4 \times 10^{-4}$

$G = 0.2$

$f = 2.8 \times 10^{13}$ Hertz

$P_{LO} = 0.3$ watts

$T_L = 300^{o}K$

$B = 2 \times 10^{6}$ Hertz

$R_L = 50$ ohms

The carrier signal-to-noise ratio for T = 1 from equation (2-4) is then

$$\frac{S}{N} = 69 \text{ dB} \qquad (2\text{-}14)$$

Factors included in the calculation of T are the transmission efficiencies of the atmospheric path and the receiver optical system. Atmospheric absorption at sea level for the 10.6 micron wavelength is about 0.1 km^{-1} at $100^{o}F$.(2-3) For the 4 km path this gives a transmission efficiency of 67%.

The receiver optical system up to, but not including, the beam combiner presents the following transmission efficiencies (starting from the receiver telescope input)

Transmission past 1" dia diagonal mirror	93%
Reflection from Au and Al coated surfaces (3 surfaces @ 98%)	94%
Transmission through kCl lens	90%
Total for receiver	79%
Total for receiver and atmosphere	53%

The signal to noise ratio after including transmission factors then becomes;

$$\frac{S}{N} = 66 \text{ dB} \qquad (2\text{-}15)$$

Other factors which must be considered include the angular misalignment between local oscillator and signal beams after being combined in the receiver, and the efficiency of the heterodyne mixing at the detector. Adjustments are available for peaking the alignment of the L.O. and signal beams. This, along with proper adjustment of the focusing optics to optimize the spot sizes on the detector element for best heterodyne mixing, makes a factor of 0.5 seem a reasonable and conservative estimate for the efficiency of the beam combining and mixing process. A carrier to noise ratio of about 63 dB is therefore expected.

SECTION 3.0
COMPONENTS FOR COMMUNICATION SYSTEM

3.1 Introduction

In Section 2, performance of the communication system was discussed and basic requirements for the components were established. The present section discusses the design and development of these components, with particular emphasis on the design and development of the laser oscillators and the electro-optic phase modulator, since they represent state-of-the-art components. Included in this section is a discussion of the operating characteristics of the CO_2 laser which will prove helpful in understanding operation of the system. Also included is a duscussion of stabilization principles and techniques appropriate to the CO_2 laser.

3.2 CO_2 Laser

3.2.1 CO_2 Laser Operating Characteristics

Optical communication systems using the CO_2 laser as a carrier source typically must use heterodyne detection at the receiver to achieve acceptable noise performance with reasonable transmitter power. In a heterodyne detection system, it is of primary concern that both the carrier and local oscillators operate at nearly the same frequency within a few tens of megahertz. Because of the CO_2 laser's ability to operate almost equally well at a number of widely spaced frequencies, special attention must be given to its operating characteristics.

As already noted, the CO_2 laser can readily operate on any of the following transitions;

$00^{\circ}1 - 10^{\circ}0$	P (even)	$\sim 10.6\mu$
$00^{\circ}1 - 10^{\circ}0$	R (even)	$\sim 10.2\mu$
$00^{\circ}1 - 02^{\circ}0$	P (even)	$\sim 9.6\mu$
$00^{\circ}1 - 02^{\circ}0$	R (even)	$\sim 9.3\mu$

Short lasers having less than a meter or so of active length (using no wavelength selective device) tend to operate at a single rotational-vibrational wavelength in any of the first three bands listed above, and, on occasion, the fourth. Strongest oscillation is obtained at wavelengths near 10.6 microns.

Within each of these bands (as previously mentioned) several closely spaced wavelengths corresponding to transitions from the rotational sub-levels can occur. For example, we have observed lasing at the following wavelengths near 10.6 microns:

P(14)	10.5322μ
P(16)	10.5519μ
P(18)	10.5716μ
P(20)	10.5915μ
P(22)	10.6119μ
P(24)	10.6327μ
P(26)	10.6537μ

An important factor in the operating characteristics of the CO_2 laser is that all of the lasing transitions have upper energy levels in the same $(00^{o}1)$ vibrational band. Due to fast relaxation occurring among energy levels in the upper band (aided by the addition of helium to the gas mixture), there is a strong tendency for an equilibrium Boltzmann distribution of excited states in the upper levels to be maintained. Therefore, when lasing action occurs from a particular upper level, all other levels begin to supply energy to that level, with the result that gain at the other wavelengths within that band is lowered. Potential oscillations at other wavelengths are thus suppressed. For this reason, short CO_2 lasers will tend to operate at a single (but largely unpredictable) wavelength.

The CO_2 laser transition lines, especially in laser tubes using relatively high partial pressures of CO_2 (between 2 and 6 torr), exhibit homogeneous line broadening in addition to Doppler (inhomogeneous)

line broadening. The Doppler component of broadening in typical discharges in both experimentally and theoretically found to be on the order of 60 MHz.[3-1] Pressure broadening contributes from 10 MHz to 30 MHz additional line broadening within this pressure range. Oscillating linewidths for CO_2 lasers of between 90 and 150 MHz have been measured[3-2]. For a laser such as those used in the present system, having a cavity length of about 0.5 meter (axial resonance interval of about 300 MHz), superposition of the comb of axial resonances over the series of gain lines near 10.6 microns would appear roughly as shown in Figure 3-1. Noteable features are that; 1) no more than a single axial mode near each transition line will experience sufficient gain to oscillate. (Even in longer lasers where two axial modes can fall well within the gain curve, competition due to the homogeneous line broadening tends to allow only one to oscillate. And, 2) as the comb of cavity resonances is tuned across the series of gain lines by adjusting the laser mirror separation, oscillation will occur at various wavelengths in a unique sequence depending on which wavelength offers the highest excess gain when the preceeding oscillation is quenched for lack of gain.

To set the laser at some desired transition frequency, it is necessary to tune the length of the laser cavity until a cavity resonance coincides with that frequency. The laser will then remain in operation at that frequency until the cavity resonance drifts far enough from the line center that another wavelength experiences higher gain and takes over. This typically occurs at about 10 to 20 MHz from line center. If however, the laser is constrained to oscillate at only one wavelength (for example, by including a dispersive element in the optical cavity), the laser can typically be tuned over the entire oscillating linewidth ($\sim \pm 50$ MHz) from line center. Tuning beyond this range simply extinquishes the laser.

We have observed that the P(20) transition at 10.59 microns gives the strongest laser output and it was therefore desirable to limit one of the lasers to oscillation at this wavelength. Acquisition of the 10 MHz i.f. signal thus ensures that both lasers are operating at this

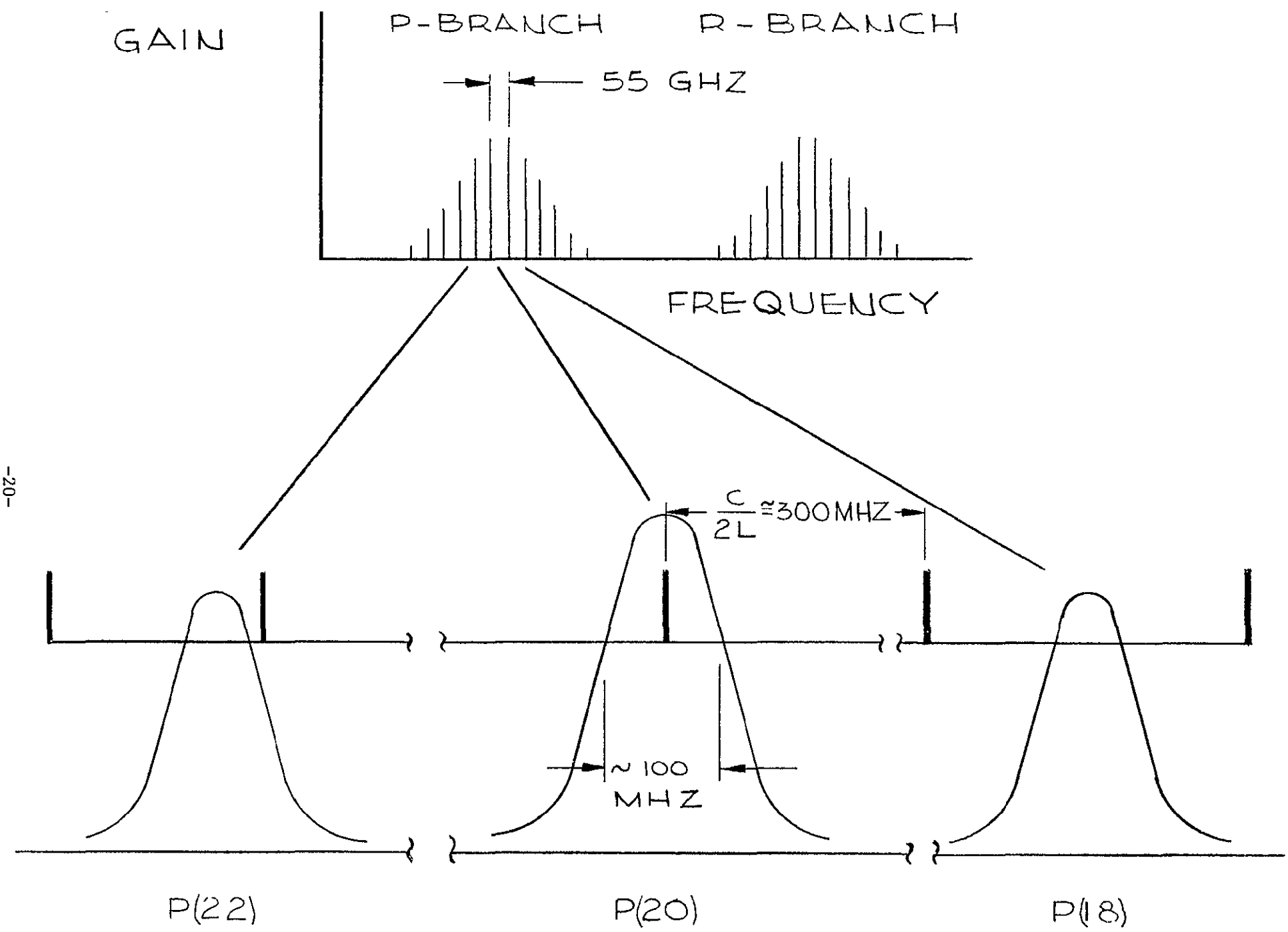

Figure 3-1. Relationship of Cavity Resonances to P(J) Gain Lines.

wavelength. This wavelength selection is accomplished by the use of a blazed reflectance grating as one of the cavity mirrors in the local oscillator laser.

Consideration of other laser operating characteristics important to the present system includes the requirement for a high degree of frequency stability to minimize noise in the communication channel. Mechanical and electrical features in the present design which provide for these requirements are discussed in the following section.

3.2.2 Laser Design

The laser oscillators in the transmitter and receiver use the same type of discharge tube and mechanical cavity structure. Laser specifications are:

1)	Output Wavelength	10.59 microns
2)	Output Power.	1.0 watts
3)	Mode Purity	TEM_{oo} Mode, Single frequency
4)	Polarization	Linearly polarized, vertical
5)	Frequency Stability	<±15 MHz long term (Hours) <± 3 kHz short-term (10 ms)

As mentioned earlier, as an aid in the initial spectral alignment of the transmitter and receiver local oscillator lasers, a grating has been used in the local oscillator to limit its operation solely to the 10.59μ line. This grating reduces the power output, however, to about 500 mW. In normal operation, the receiver and transmitter lasers are locked together by an AFC loop, so the long-term frequency stability requirements apply only to the transmitter laser. The magnitude of the frequency drift must be limited to about ±15 MHz in order to keep the transmitter oscillating on the 10.59μ line. A wavelength selector was

was not used in the transmitter, so its power output was not reduced as was the LO laser's.

The following paragraphs discuss the design details of the lasers.

3.2.3 Mechanical Design

In order to achieve the frequency stability requirements, the laser cavity must be constructed to reduce the effects of ambient vibration and thermal variations on the output frequency of the laser.

In order for a structure to be stable against vibration, it is necessary that the mechanical resonances of the structure not be at frequencies within the gain power spectrum of acoustical and mechanical vibration noise inputs.

The main power spectrum of both acoustic and mechanical vibration noise is at low frequencies. The peak of the acoustic spectrum usually occurs at less than 500 Hz. In both types of noise, however, there will be occasional shocks with frequency components of up to perhaps 30 kHz. The fact that most of the noise power spectrum for vibrational excitation occurs at low frequencies, together with the fact that high frequency noise is easier to isolate from a structure than is low frequency noise, dictates that the CO_2 laser structure should be designed to make the structural frequency resonances as high as can be achieved.

The frequency of the lowest longitudinal resonance of a laser cavity structure is determined by the cavity length. This frequency is given by the equation

$$f_{L\nu} = \frac{C_s}{2L}$$

where C_s is the velocity of sound in the structure, and L is the structure length.

In choosing a length for the CO_2 laser, one must make a trade-off between high longitudinal-mode frequency and stiffness against bending distortion on the one hand and high output power on the other. Assuming a structure made of invar for thermal stability reasons, Table 3-1 shows the lowest longitudinal frequency for various cavity lengths.

Table 3-1

Lowest Longitudinal Mode Frequencies in Invar Laser Cavities

Cavity Length	Frequency
1 m	2 kHz
50 cm	4 kHz
20 cm	11 kHz
10 cm	21 kHz

A 50 cm long cavity length was chosen for this program as being able to provide substantial output power (about 1 watt single frequency) while still maintaining lowest-order resonant frequencies high enough that substantial vibrational damping can be applied.

The design of the remaining structure was then chosen to avoid lowering the basic first resonance. The individual elements of the structure were chosen with geometries and methods of support (boundary conditions) such that they do not have low frequency transverse resonances. The joints between the elements of the structure were also designed so that they do not have any low frequency resonances. Especially critical are the joints perpendicular to the cavity length. One particularly good design for these joints is to use large contact areas under compressional stress. The spring constant of the joint will then be high. Designs with joints using only the spring force of a few screws to connect significant masses have been avoided.

The cavity consists of a rigid channel-shaped structure with the laser tube mounted in the channel and the mirror mounts clamped to the ends.

The channel-shaped structure was chosen because of its high resistance to bending deformation. When the lid is attached and the fourth side of the structure closed, the resistance to bending is almost identical to a cylindrical structure (optimum for resistance to bending) of similar cross-sectional dimensions. However, the rectangular structure allows much easier access to the cavity.

In order to conserve weight but still maintain the required thermal characteristics (as explained in later paragraphs), the channel-shaped cavity was constructed primarily from aluminum, with invar rods embedded in the aluminum. The four invar rods (located at the corners of the channel) serve as mounting points for the mirror assemblies. The rods are potted into the aluminum frame so as to provide an intimate contact between the invar and the rigid aluminum structure.

To remove the problems associated with weak spring-type controls, the mirror holders have been ruggedly designed. As can be seen in Figure 3-2, the mirrors can be adjusted in angle by sliding two mating spherical joints with respect to one another. As the mirrors are being adjusted into their final position, the adjustment screws clamp the mirror holder tightly so that no inadvertent movement is possible. The invar rods to which the mirror holders are tightly bolted are slightly longer than the aluminum cavity structure, so the mirror mounts do not contact the aluminum.

The laser tube has been mounted in the cavity with a foam insert which provides good transverse stability while offering high impedance to vibrations which may be coupled to the cavity by the coolant flowing around the laser tube.

To further reduce the intensity of airborne acoustic waves reaching the laser oscillator, the laser is covered with type Y-9052 industrial vibration damping material made by 3 M Company. This material is a pressure-sensitive specially-compounded polyurethane acoustic damping foam with an aluminum foil paper laminant constraining layer backing. The laminant

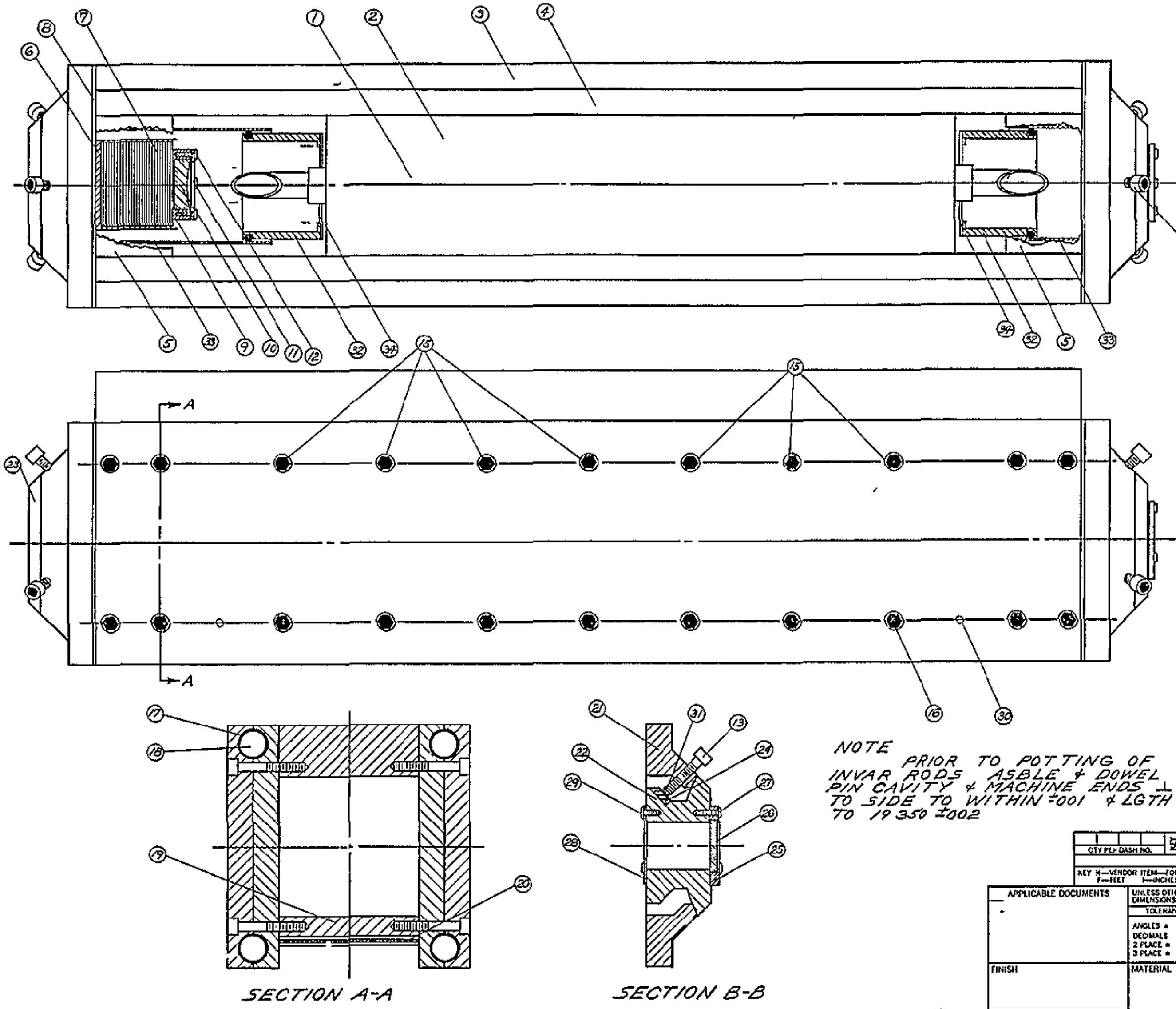

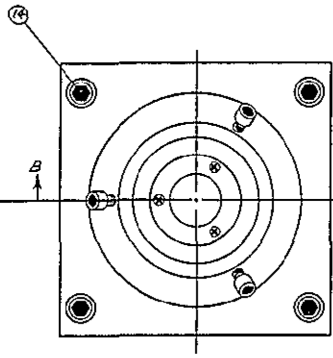

NOTE
PRIOR TO POTTING OF INVAR RODS ASBLE & DOWEL PIN CAVITY & MACHINE ENDS ⊥ TO SIDE TO WITHIN ±.001 & LGTH TO 19.350 ±.002

QTY	PART OR IDENTIFYING NO	SYLVANIA PART NO	NOMENCLATURE OR DESCRIPTION	NOTE	ITEM NO
2	9471421		NEOPRENE SEAL		34
1 EA	4780203-1&2		BOOT FLANGE		33
2	4780204		BOOT SEAL		32
3	PL-478000		BALL BEARINGS		31
4	PL 478000		DOWEL PINS		30
3	PL-478000		APERTURE SCREWS		29
1	4780194		APERTURE		28
3	PL-478000		BEZEL SCREWS		27
1	PL-478000		TRANSMISSION MIRROR		26
1	4780193		TRANS MIRROR BEZEL		25
6	PL-478000		CARBIDE INSERTS		24
1	4780192-2		SPHER. OPTICS HLDR		23
1	4780192-1		SPHER. OPTICS HLDR.		22
2	4780191		SPHER. END PLATE		21
1	4780190		HEATER		20
1	4780189		CAVITY BASE		19
4	4780188		INVAR RODS		18
	PL-478000		EPOXY		17
30	PL-478000		CAVITY BOLTS-LONG		16
14	PL-478000		CAVITY BOLTS-SHORT		15
8	PL 478000		END PLATE BOLTS		14
6	4780187		ADJ. SCREW		13
4	PL-478000		BEZEL SCREWS		12
1	9471023		BEZEL		11
1	9471022		OPAQUE MIRROR		10
1	9471024		HOLDER		9
2	9471007		EXPANSION PLATE		8
1	9471011		PIEZO-ELECT TRANSDUCER		7
1	9471006		INSULATOR		6
2	4780186		CAVITY SUPPORT		5
2	4780185-2		CAVITY - INNER SHELL		4
2	4780185-1		CAVITY - OUTER SHELL		3
1	4780184		FOAM TUBE MT		2
1	4780510		TUBE ASSY		1

PARTS LIST

KEY V—VENDOR ITEM—FOR PROCUREMENT OR PART NUMBER SEE SPECIFICATION CONTROL OR SOURCE CONTROL DRAWING
F—FEET I—INCHES B—BULK AR—AS REQUIRED

APPLICABLE DOCUMENTS | FINISH | NEXT ASSEMBLY | MODEL

UNLESS OTHERWISE SPECIFIED DIMENSIONS ARE IN INCHES
TOLERANCES: ANGLES ± DECIMALS 2 PLACE ± 3 PLACE ± | SURFACES √ MICRO-INCHES | MATERIAL

DR W. Hill | CHK | APPD | APPD

SYLVANIA ELECTRONIC SYSTEMS
DIVISION OF SYLVANIA ELECTRIC PRODUCTS INC
MOUNTAIN VIEW CALIFORNIA

CAVITY ASSEMBLY

SIZE D | CODE IDENT 0739T | 4780522
SCALE 1/1 | SHEET OF

REVISIONS: ZONE | LTR | DESCRIPTION | DATE | APPROVED

Figure 3-2 Laser Cavity Assembly

structure is especially effective for vibration isolation and it also serves as an effective thermal shield to help maintain a uniform and controllable temperature within the laser enclosure. A photograph of the laser is shown in Figure 3-3.

Although the requirement for high-frequency stability is only applicable for relatively short periods of time, the laser must be stable enough to operate continuously within the central portion of the laser gain curve. This is necessary to ensure constant power and single-wavelength operation. The length stability required to achieve the desired frequency stability of ±15 MHz is given by

$$\frac{\Delta L}{L} = \frac{\Delta f}{f} = \frac{\pm 15 \text{ MHz}}{3 \times 10^{7} \text{ MHz}} = \pm 5 \times 10^{-7} = \alpha \Delta T$$

Even using invar as the cavity separators ($\alpha = 1.0 \times 10^{-6}/^{o}C$), temperature control to about $\pm 1/2^{o}C$ is still required.

To achieve the desired temperature stability, a d.c. proportional temperature controller was constructed for use with the laser. Figure 3-4 is a circuit diagram of the control unit. A temperature-sensing thermistor used in one leg of a balanced bridge circuit produces an unbalanced condition in the bridge circuit when the enclosure temperature deviates from the set point. A dc differential amplifier amplifies the unbalanced potential caused by the thermistor and provides an input to a two-stage transistor driver. A heating coil mounted on the bottom of the laser structure and connected between a dc heater power supply and collectors of the driver transistors generates heat as demanded by the sensor. A potentiometer at the input of the driver provides a temperature adjustment for the circuit. Since the heater is located near the invar cavity mount, the heater dc supply is well filtered so that low frequency magnetostrictive effects exhibited by the invar cannot be excited. Figure 3-5 is a photograph of the temperature controller.

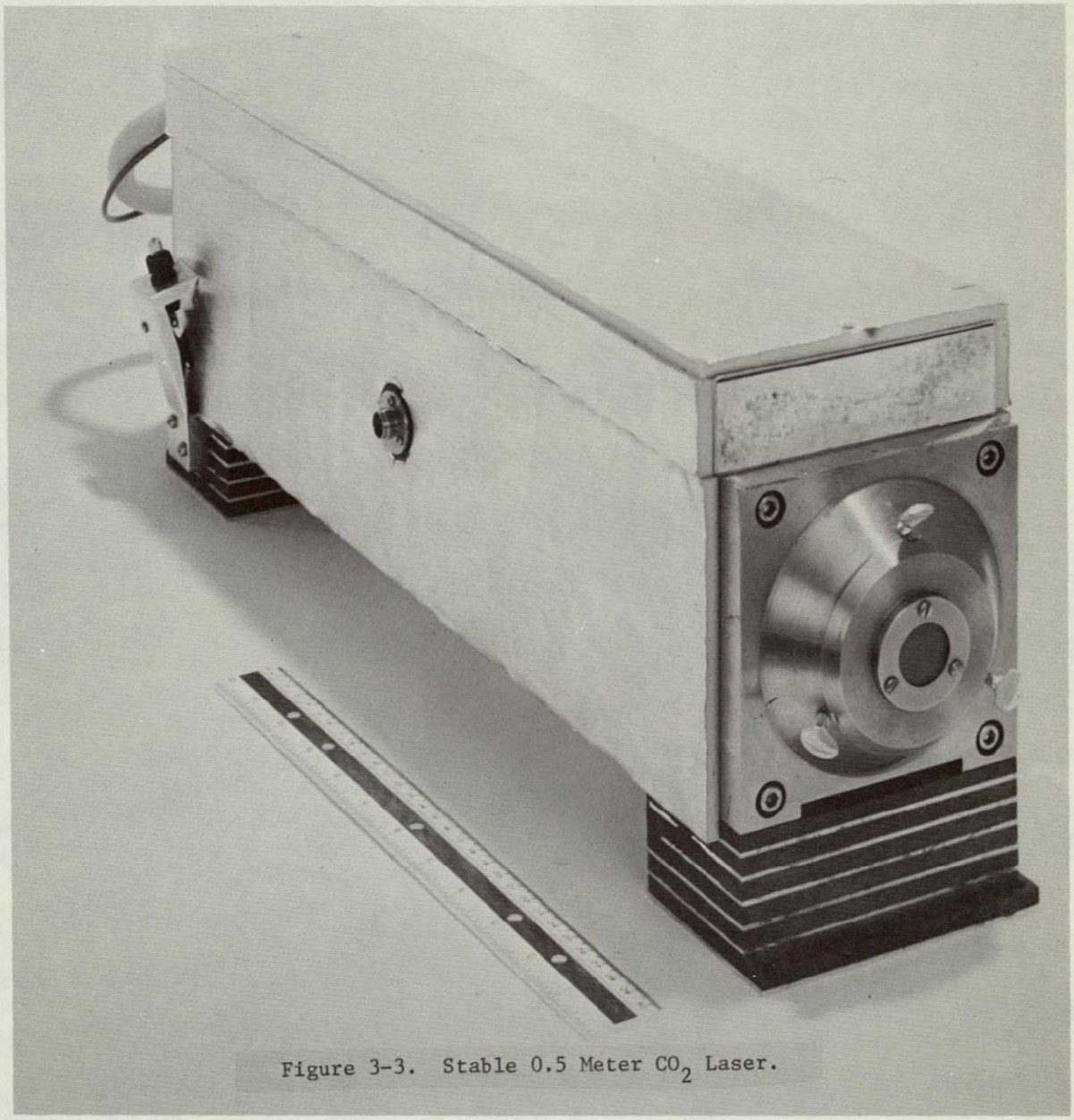

Figure 3-3. Stable 0.5 Meter CO_2 Laser.

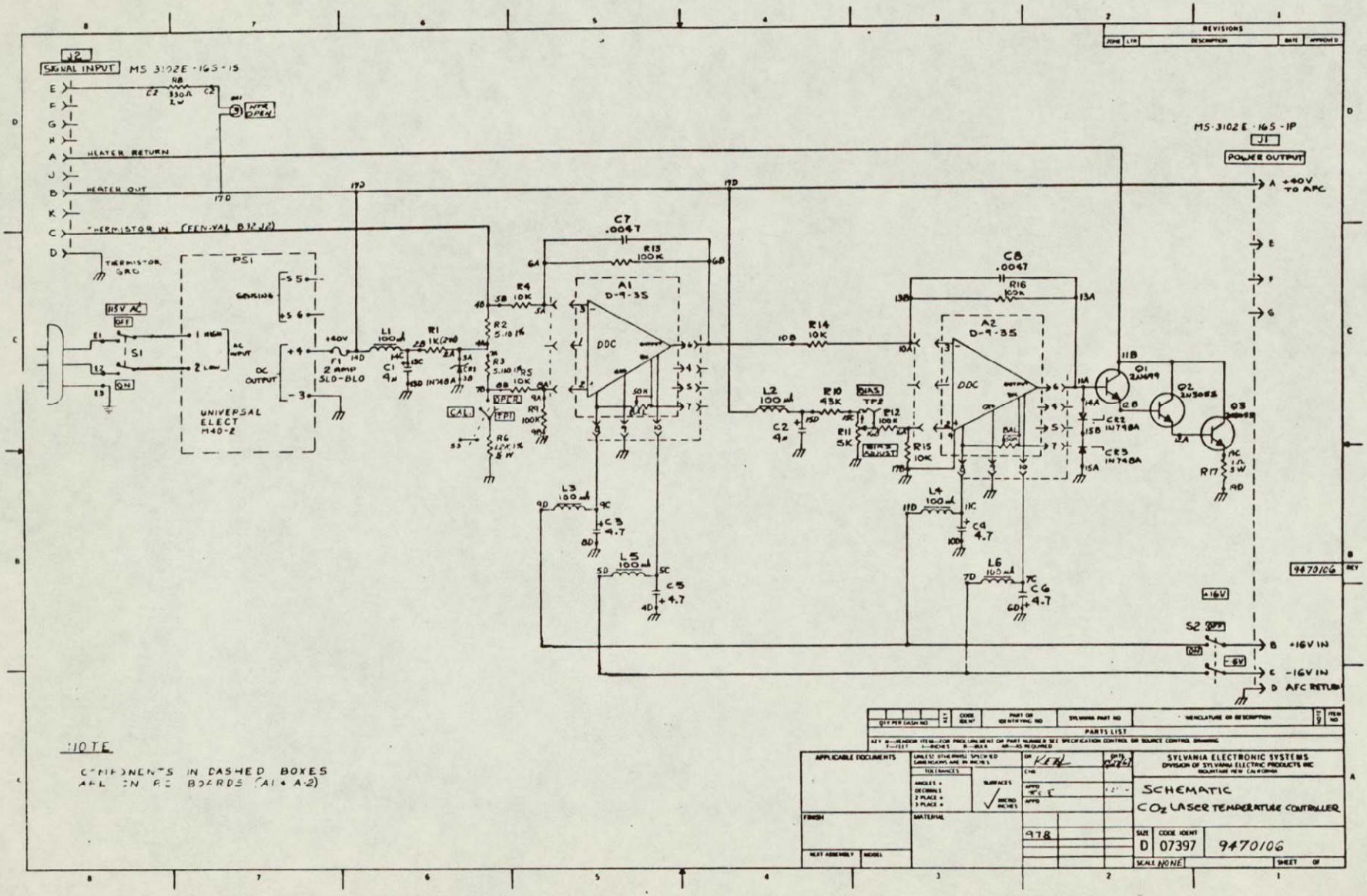

Figure 3-4. Schematic of CO_2 Laser Temperature Controller

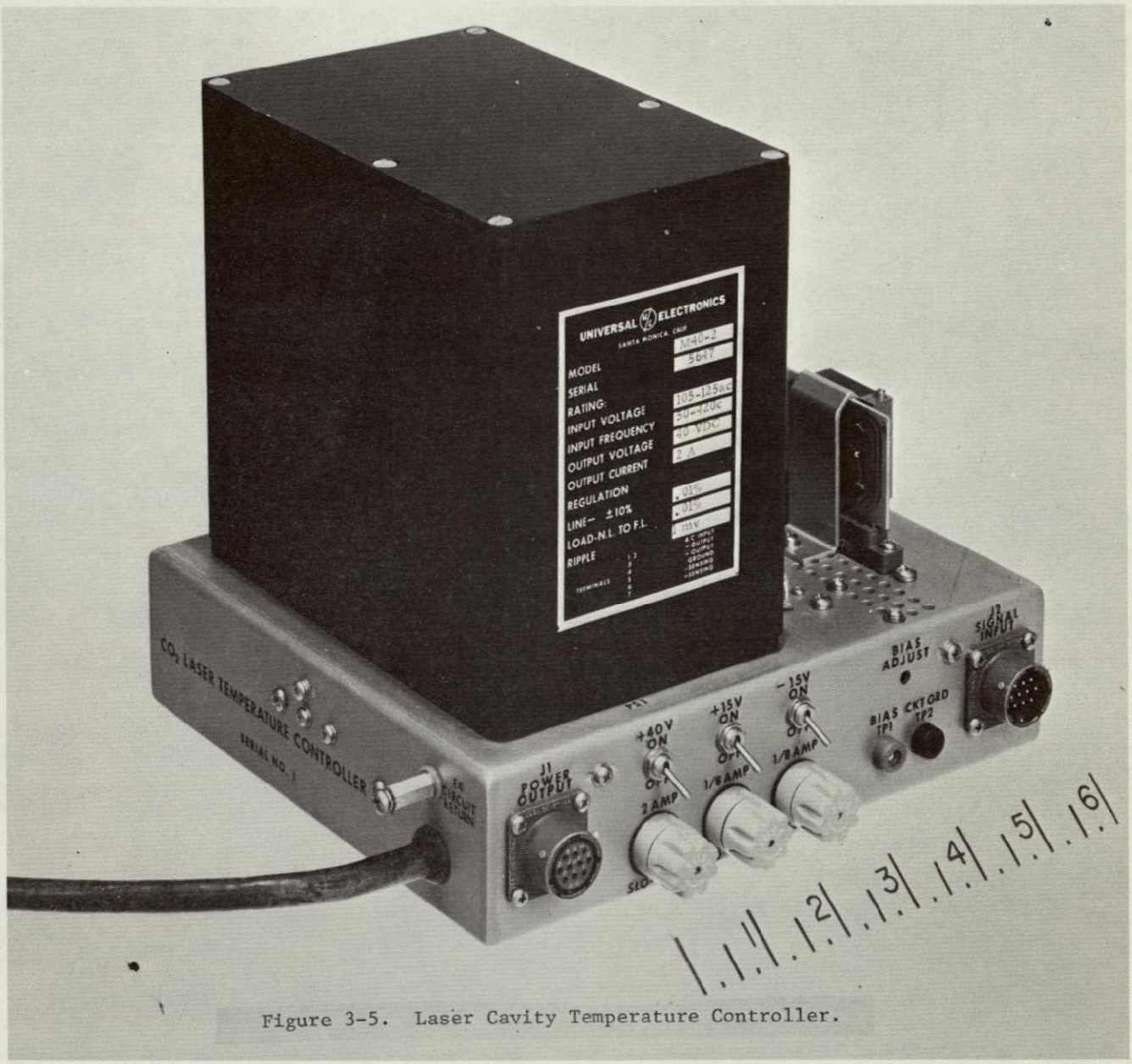

Figure 3-5. Laser Cavity Temperature Controller.

3.2.4 Plasma Tube Design

During the course of the program, several tube geometries were constructed. All had approximately the same total length and all had Brewster angle windows, although not all of the windows were the same type material.

The tubes used in the final packages were constructed from Pyrex glass. They have an active bore diameter of approximately 6 mm with an overall bore length of approximately 30 cm. It was found that in the testing of various tubes with different bore sizes, the diameter bore consistently gave high power output in a single mode. Larger-bore tubes (on the order of 8-10 mm) quite often ran with second order or third order modes mixed to some degree with the lowest-order mode. In some cases, however, the 6 mm bore tube can also run in a TEM_{01}^{*} mode, requiring the use of an intra-cavity aperture. At intervals of about 4 cm, the bore diameter has been slightly reduced, forming a small ripple. This has been found important in eliminating spurious modes of oscillation in which the glass bore acts as a reflector for very low incidence angles. This feature is particularly important when a dispersive wavelength selector (e.g. grating end reflector) is used with the laser. There is a very great tendency, otherwise, for unwanted wavelengths to lase in a mode which involves reflection from the bore.

The Brewster angle windows used in the tubes were constructed from high resistivity (1×10^{8} Ω-cm) GaAs. The absorption coefficient of this material was measured to be approximately the same as the best optical grade germanium (.01 per cm) but GaAs does not suffer the thermal runaway problem to the extent that germanium does. Because of the high refractive index of the GaAs material ($\sim$3.2) it was necessary to fabricate windows having a very high quality surface figures; otherwise severe mode distortion would occur. The window surfaces were polished flat to within 1 or 2 fringes (visible wavelength) in order to avoid this distortion.

Use of the GaAs material for Brewster windows has proven much more satisfactory than use of either NaCl or KCl for several reasons: The GaAs material is not hygroscopic and is unaffected by high humidity conditions (unlike the salt materials.) GaAs has much greater mechanical strength than the salt materials, allowing the windows to be sealed to the tube with high-vacuum epoxy. Stresses produced by this epoxy usually crack KCl or NaCl windows.

These tubes use a nickel cathode which was constructed in a re-entrant cylindrical configuration. The discharge was run from the inside diameter of the cathode so that sputtering from one portion of the cathode could be deposited on the other side, allowing re-sputtering and liberation of any trapped gases buried by the sputtering process. In all cases, the anode was simply a tungsten pin.

The tube also used a reservoir volume of approximately 1/5 liter. Since the laser tube was water-cooled, the ballast resistors used with the tube were also placed in a water-cooled jacket. This allowed a much smaller size resistor string to achieve the same power dissipation capability.

For the above size bore and length of the laser tube, the optimum current and voltage for the laser was approximately 9.5 kV at 11 milliamperes. Powers ranging up to 1.5 watts were observed from this laser when an 8% transmission output mirror was used. The above powers were obtained with a gas mixture of 1.5 torr Xe, 5 torr CO_2, 2 torr N2, and 18 torr He. The Xenon was used to achieve lower operating and breakdown voltages.

3.3 GaAs Phase Modulator

The modulator in the present system makes use of the electro-optic effect in GaAs to produce phase modulation of the 10.6 micron laser beam. GaAs is a cubic crystal having $\bar{4}3m$ symmetry, the same class as ZnS, CuCl, GaP, CuBr, ZnTe and ZnSe. Excellent references exist[3-3, 3-4],

which discuss in detail application of the theory of the linear electro-optic effect to crystals in this symmetry class. For the present phase modulator the GaAs crystal orientation was chosen so that the light propagates in the $|\bar{1}10|$ crystal direction and the electric field is applied perpendicular to the propagation direction by electrodes in (110) planes. When the modulator is oriented so that the polarization of the optical beam is at 45^{o} to the applied electric field, phase modulation is impressed on the optical signal, with phase deviation related to the applied voltage by

$$\Delta\phi = \frac{\pi\, n^3\, r_{41}\, V\, L}{\lambda d} \quad ,$$

where n is the refractive index of GaAs, r_{41} is the electro-optic coefficient involved, V is the voltage applied across the crystal thickness d, and L and λ are respectively the crystal length and the laser wavelength.

The modulator uses two rods, giving a combined length of about 9.6 cm. The width of the rods is 0.3 cm (square section). Using these figures and the material constants[3-5]

$$n = 3.3$$

$$r_{41} = 1.6 \times 10^{-12} \text{ m/V}$$

gives

$$\Delta\phi = 0.55 \text{ radian/kV}$$

The signal supplied by the broadband modulator driver described in the following section is limited to 400 V peak by the present state of the art in high voltage power transistors. Maximum phase modulation depth for the present system is therefore 0.22 radians.

It is of importance later to note that the particular crystal orientation used is not the one which affords the maximum phase retardation for a given crystal size and voltage; it is about 14% poorer than the

optimum orientation for phase modulation. It does, though, provide the maximum phase retardation between orthogonally polarized light waves, so the modulator can very easily be converted to a polarization modulator by using a $\lambda/4$ wave plate in front of the modulator. This allows added flexibility in that the communication system can be quickly converted from phase modulation to AM, and vice versa. The AM in this case is produced by the fact that the heterodyne interaction at the receiver is sensitive to relative polarization angle between the signal and local oscillator beams. The AM modulation depth available by this technique for the present system is calculated to be about 0.19.

Figure 3-6 is a photograph of the modulator assembly showing the three-axis rotational adjustment possible with this mount. The upper and lower electrodes are both insulated from ground and are constructed to provide low capacitance to ground, thus reducing the amount of modulator drive power required.

KCl lenses are provided at the input and output ports of the modulator to focus the 6 mm diameter beam into the 3 mm square rods and then re-collimate the beam again at the output. Focal length for the lenses is 4.1 cm.

Due to the piezoelectric effect in GaAs, an applied electric field at the proper frequency can excite mechanical resonances of the modulator crystals. For the particular geometry of the present modulator, a strong mechanical resonance exists at 690 kHz. Figure 3-7(a) shows the modulation depth obtained with just 10 V (peak) applied to the modulation depth is approximately 2, representing an increase in peak phase shift per volt of about 400 times over the off-resonance value. Figure 3-7(b) shows the sideband picture after clamping the modulator rods between lead electrodes to absorb the mechanical energy. The modulation depth for the same applied signal is approximately 0.16, still very near the modulation depth obtained with 400 volts (peak) applied at off-resonance frequencies. As will be seen in Section 4,

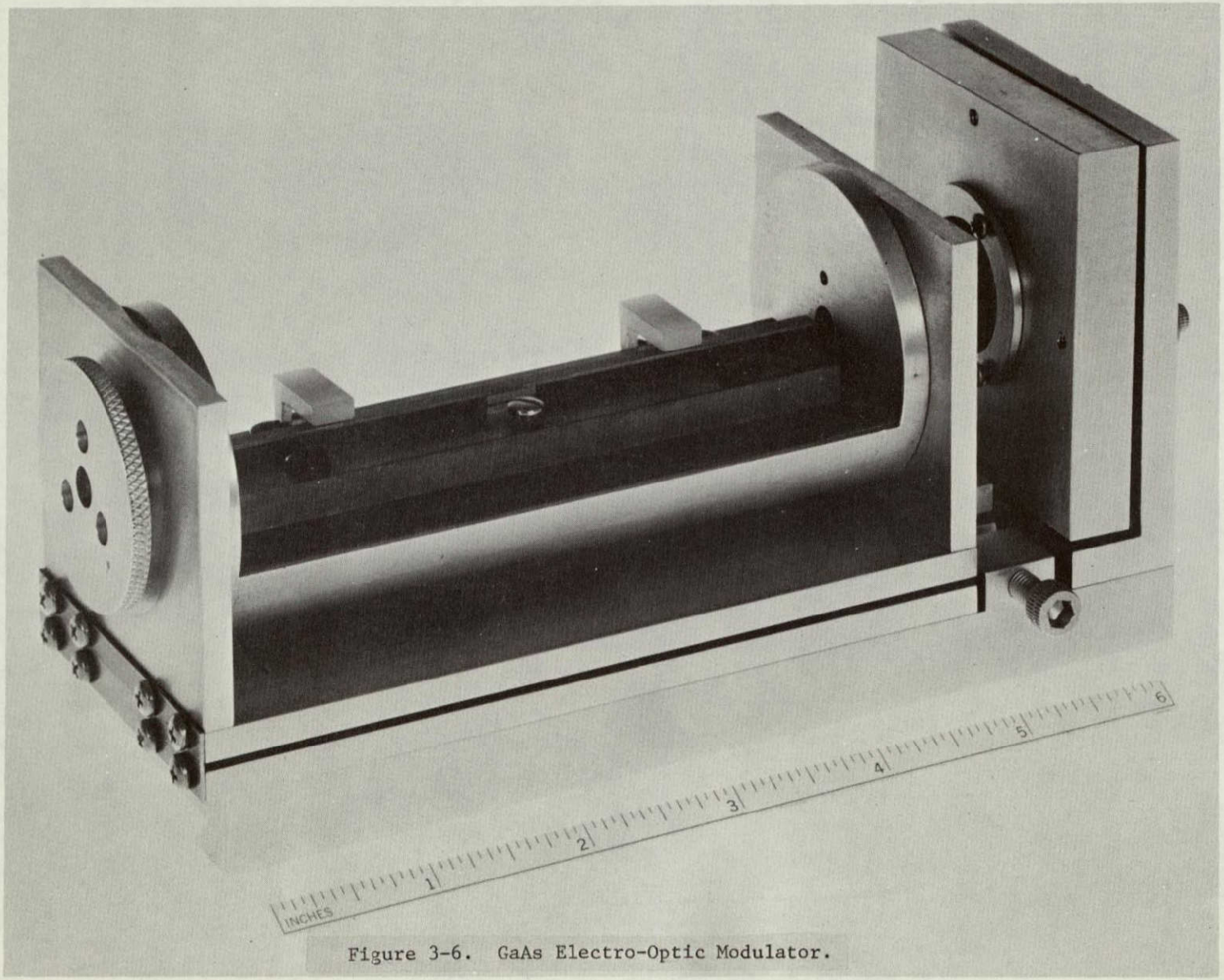

Figure 3-6. GaAs Electro-Optic Modulator.

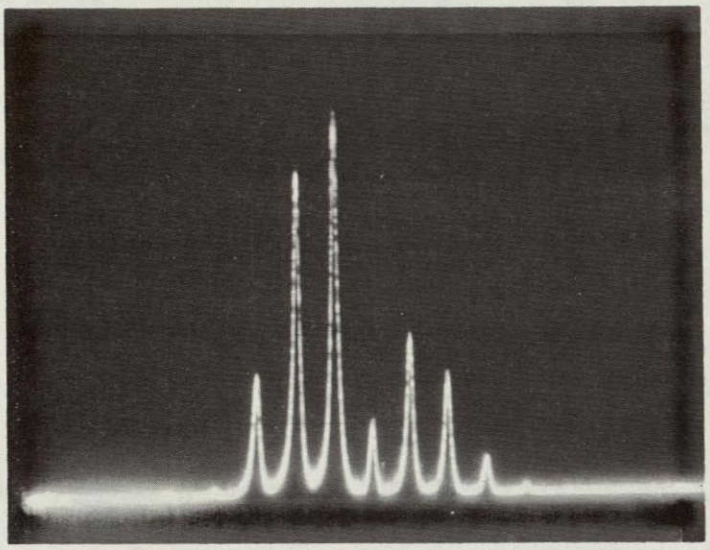

(a)

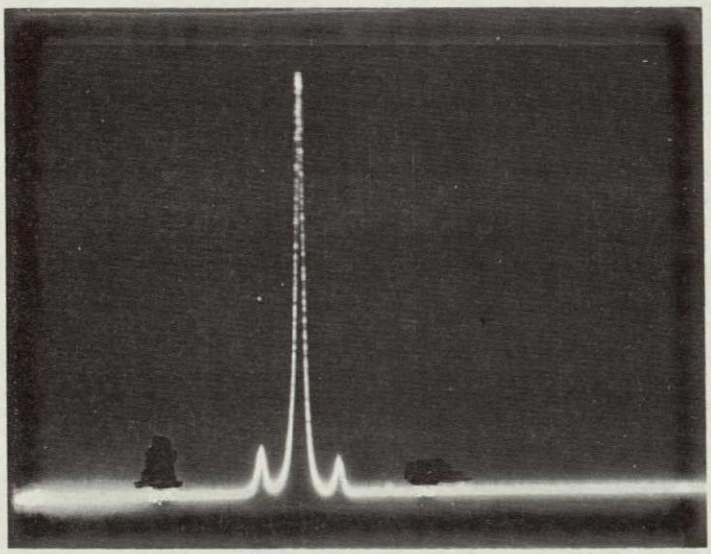

(b)

Figure 3-7. Phase Modulation Sidebands Before (a) and After (b) Clamping Modulator Rods in Lead. Modulation Voltage = 10 V (peak) at 690 kHz.

this effect is still far too strong to be acceptable in broadband communications. Further work on the modulator will be required to eliminate the effect. In addition to clamping the rod between lead electrodes, it will be helpful to clamp the sides with a suitable dielectric material as well.

3.4 Modulator Driver

The driver circuit used to supply the 400 V (peak) signal to the modulator is shown schematically in Figure 3-8. The circuit consists of two class A output stages (Q1 and Q2) which are driver 180° out of phase from each other by Q3 and Q4. The output transistors are operated in the grounded base configuration to minimize the effect of transistor output capacitance (Miller effect) and to take advantage of the higher breakdown voltage available in this configuration. Each output signal has an amplitude of 200 volts, so that by applying the signals respectively to the ungrounded upper and lower electrodes of the modulator, a peak voltage across the modulator of 400 volts is obtained.

The load seen by each output stage is very nearly a pure capacitance which includes approximately 10 pf due to the modulator plus 20 pf of transistor and stray capacitance. In order to obtain frequency response out to 2 MHz, it is necessary to charge the capacitance through a collector load resistance of 2500 ohms. With the collectors of Q1 and Q2 biased at 200 volts, the power dissipation in each load resistor and each transistor becomes 16 watts, for a total dissipation of 64 watts. This power is absorbed by water cooling the heat sink plate within the driver package. The same water that cools the laser is used and the water-flow interlock prevents operation of the modulator when no water is flowing.

The Fairchild μA 733 differential video amplifier shown in Figure 3-8 provides the split phase signals to Q3 and Q4 from a single input terminated by 1 kilohm. An external input signal amplitude of 0.5 volts provides the full 400 volt output over the midband range. Frequency response is as shown in Figure 3-9.

A photograph of the driver is shown in Figure 3-10.

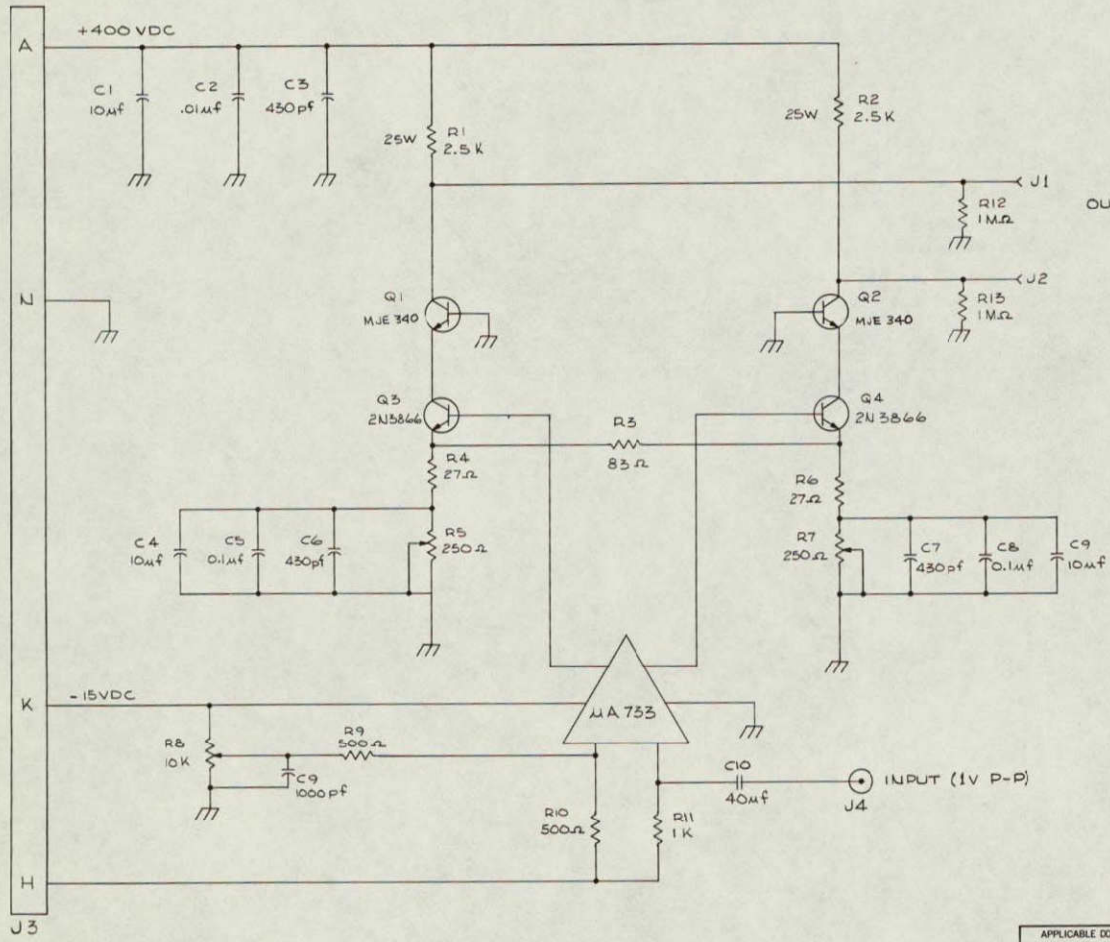

Figure 3-8. Schematic Diagram of Broadband Modulator Driver.

REVISIONS				
ZONE	LTR	DESCRIPTION	DATE	APPROVED

QTY PER DASH NO.	KEY	CODE IDENT	PART OR IDENTIFYING NO.	SYLVANIA PART NO.	NOMENCLATURE OR DESCRIPTION	NOTE	ITEM NO.

PARTS LIST

KEY: X—VENDOR ITEM—FOR PROCUREMENT OR PART NUMBER SEE SPECIFICATION CONTROL OR SOURCE CONTROL DRAWING
F—FEET I—INCHES B—BULK AR—AS REQUIRED

APPLICABLE DOCUMENTS	UNLESS OTHERWISE SPECIFIED DIMENSIONS ARE IN INCHES TOLERANCES ANGLES ± DECIMALS 2 PLACE ± 3 PLACE ±	SURFACES MICRO INCHES	CONTRACT NO. DR Tom Cole DATE 8/18/69 CHK APPD	SYLVANIA ELECTRONIC SYSTEMS DIVISION OF SYLVANIA ELECTRIC PRODUCTS INC MOUNTAIN VIEW, CALIFORNIA
FINISH	MATERIAL		APPD RELEASE APPD BY	A1 MODULATOR DRIVER
NEXT ASSEMBLY / MODEL				SIZE D / CODE IDENT NO. 07397 / DRAWING NO. 478-0535 SCALE — / SHEET 1 OF 1

SES-W-1756 (5-68)

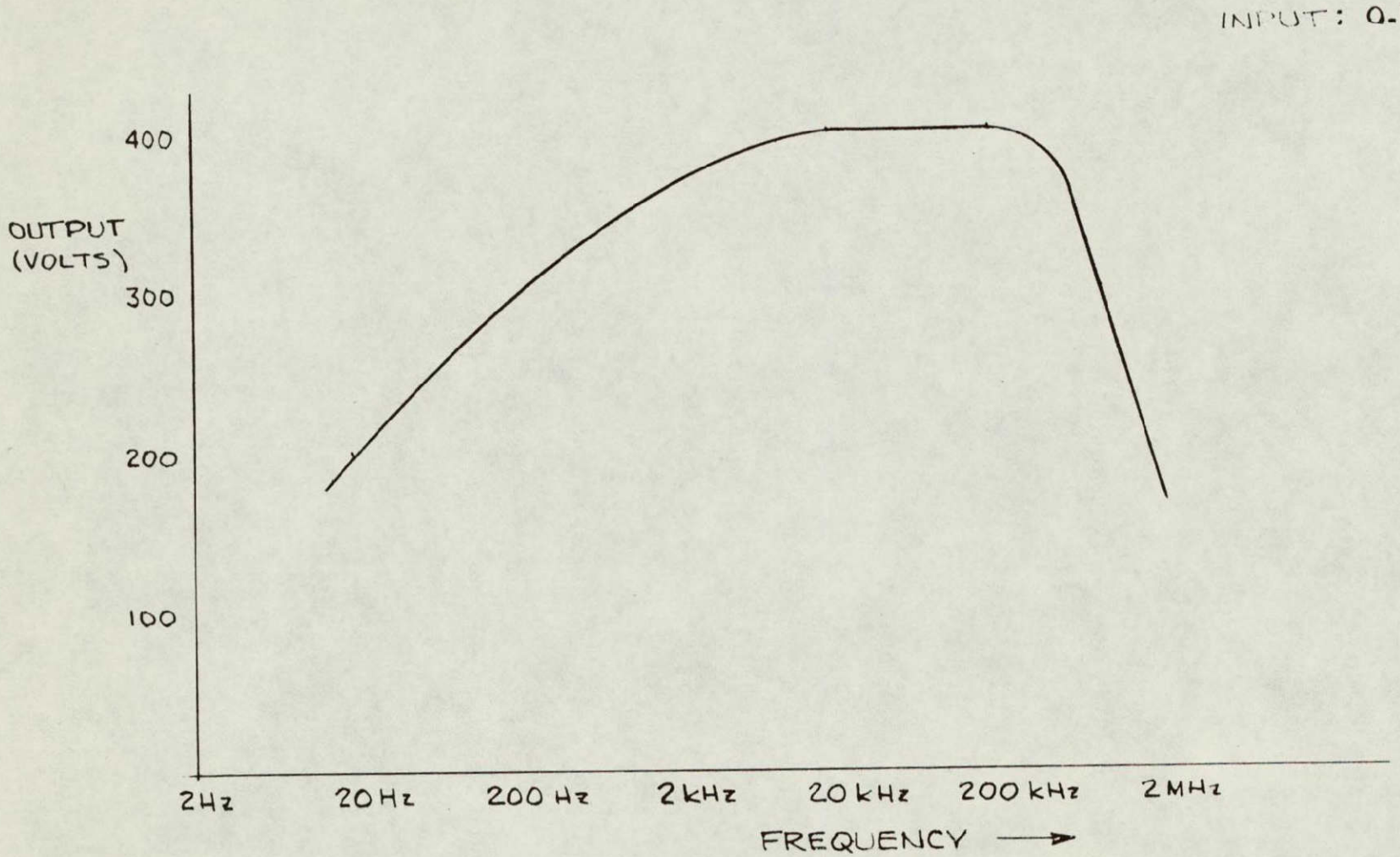

Figure 3-9. Modulator Driver Frequency Response.

Figure 3-10. Phase Modulator Driver.

3.5 Telescope

The telescopes used on the transmitter and receiver units are identical Newtonian types, both making use of 4 1/4 inch diameter parabolic aluminized primary reflectors having a 19 inch focal length. These mirrors were made by Cave Optical Co., Long Beach, California. The secondary is a single-element KCl lens having a focal length of 3.2 cm in order to match the 4 1/4 inch telescope diameter and 6 mm laser beam diameter. The telescope appears in photographs of the total system later in this section.

3.6 Receiver Electronics

3.6.1 Introduction

As previously mentioned, the receiver performs heterodyne detection of the phase-modulated 10.59 micron carrier signal. By combining the received signal with a signal from the 10.59 micron local oscillator laser, frequency translation of the 2 MHz wide information band to a 10 MHz i.f. is accomplished. This 10 MHz i.f. is maintained by an AFC loop which keeps the frequency of the local oscillator laser offset from the transmitter laser frequency by 10 MHz.

Due to the difficulty involved in phase locking, the local oscillator laser at this 10 MHz offset, it is not possible to use direct phase detection of the incoming phase information. Instead an FM discriminator is used to detect rate of change of the carrier phase. This is followed by an electronic integrator to restore the receiver output to an analog of the modulation signal. Figure 3-11 is a block diagram of the principal components used in the receiver. Their location in the receiver system is shown in Figure 3-12.

3.6.2 Detector

The 10.6 micron photodetector used in the receiver is a gold-doped germanium photoconductor made by Santa Barbara Research Center. The detector is cooled to $77^{o}K$ by liquid nitrogen when in use, and the

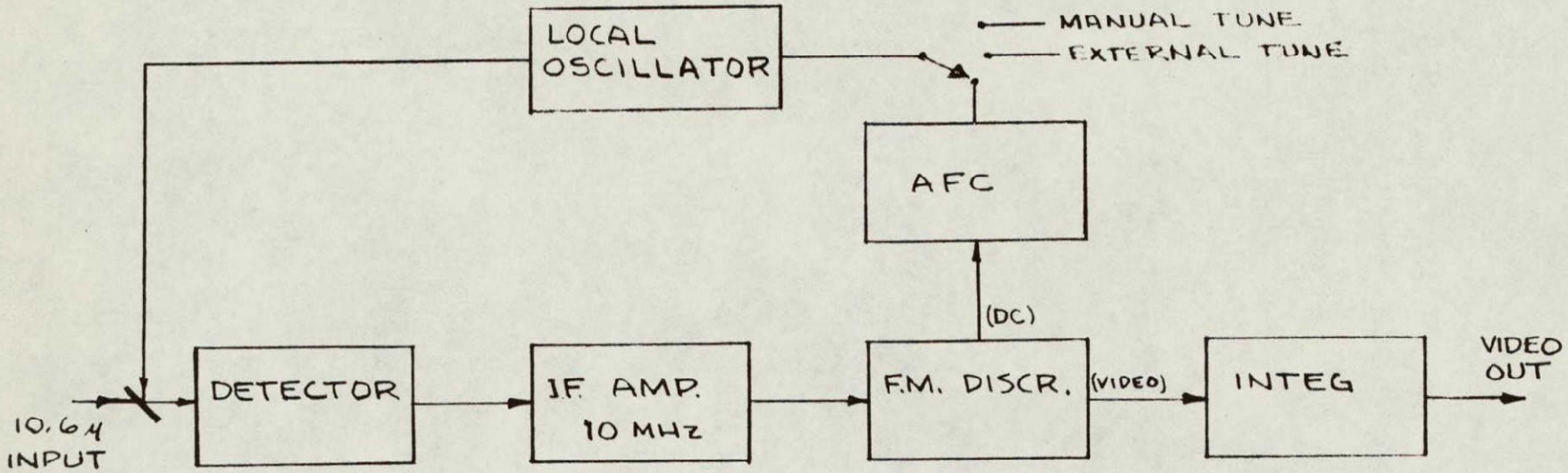

Figure 3-11. Block Diagram of Receiver.

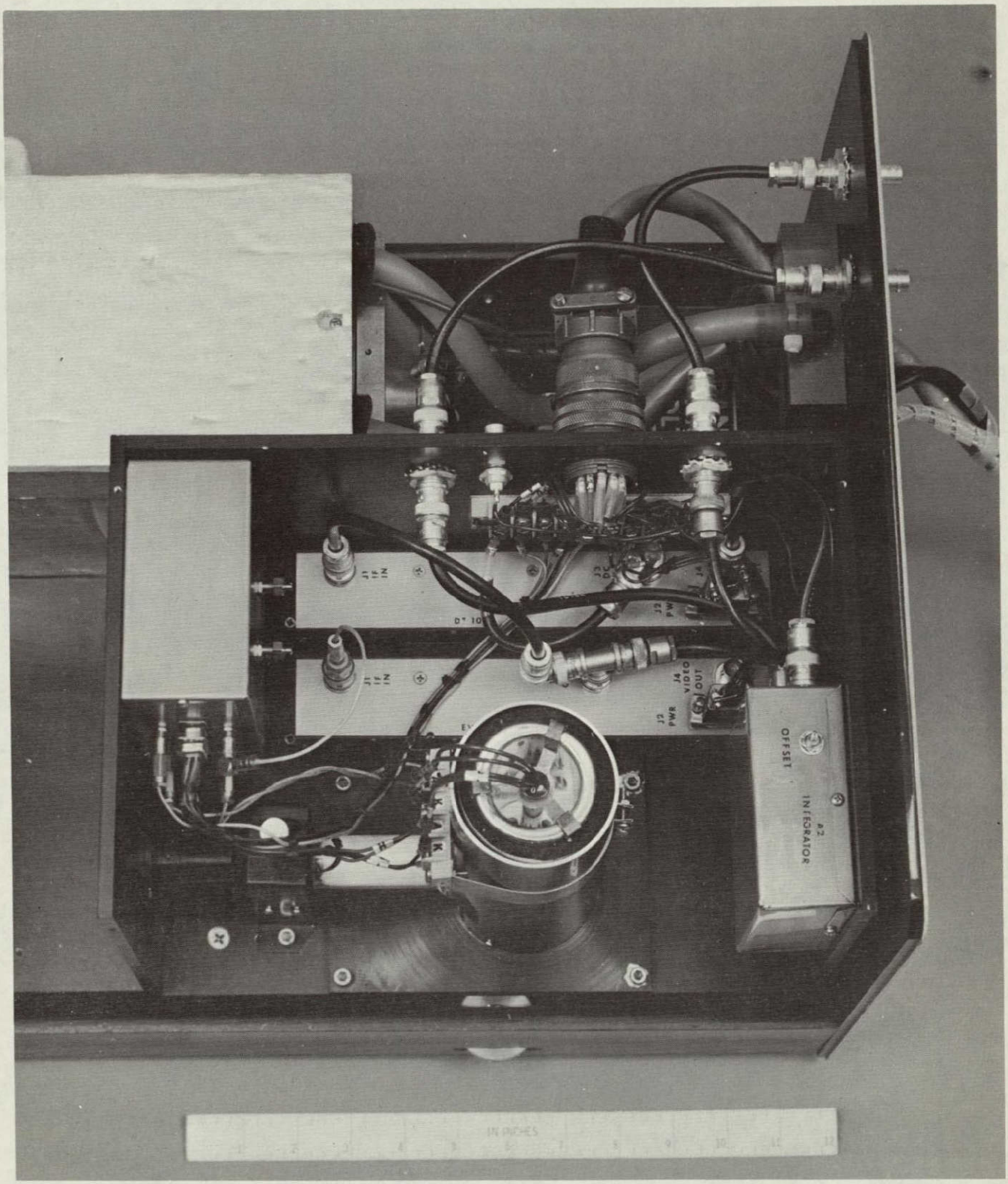

Figure 3-12. Photograph of Laser Receiver Electronics.

dewar used with the detector is nominally capable of holding LN_2 for 4 hours. The sensitive area of the detector is 0.2 mm^2 (0.5 mm dia) located behind an Irtran-2 window.

Although this detector is not ideally matched to the 10.6 micron wavelength, it does allow reasonable performance in a heterodyne system with sufficient local oscillator power, as is available in the present case. Parameters of interest for the detector have been calculated for the 10.6 micron wavelength from data supplied by the manufacturer:

Table 3-2

Detector Specifications

$D^*_{10.6} = 2 \times 10^7 \quad \frac{cm\ (Hz)^{1/2}}{watt}$
quantum efficiency = 0.04%
photoconductive gain = 0.2

Bias for the detector is supplied by a regulated voltage derived from the laser temperature controller power supply. Both electrical and optical power to the detector are interlocked so that neither is on unless the detector is cold. Figure 3-13 is a schematic diagram showing the detector bias and interlock circuit.

3.6.3 I.F. Amplifier and F.M. Limiter-Discriminator

The 10 MHz i.f. amplifier and F.M. discriminator used in the receiver are standard components produced by RHG Electronics. The I.F. amplifier is a type EVT 1002 having the following specifications.

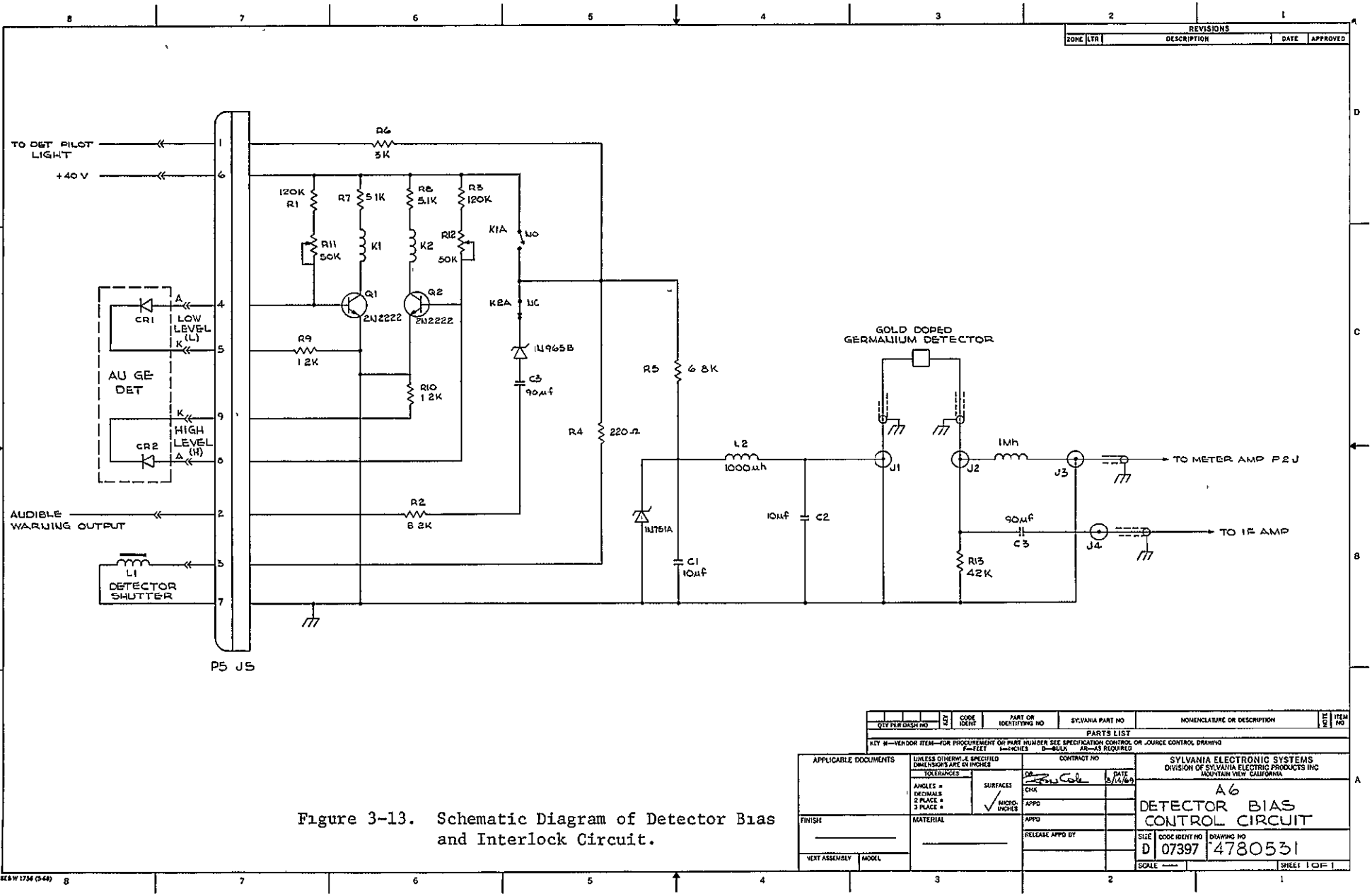

Figure 3-13. Schematic Diagram of Detector Bias and Interlock Circuit.

Table 3-3

I.F. Amplifier Specifications

center frequency	10 MHz
bandwidth	2 MHz
noise figure	2.5 dB
max. power gain	82 dB
max. voltage gain	101 dB
max. voltage output	7 volts
power required	+12 VDC, 110 mA

The limiter-discriminator is a type DT 1004 having specifications shown in Table 3-4.

Table 3-4

FM Limiter-Discriminator Specifications

center frequency	10 MHz
peak to peak bandwidth	6 MHz
video output	1.5 volts/MHz
D.C. output	160 mV/MHz
power required	±12 VDC, 80 mA

Full limiting in the limiter-discriminator occurs at 0 dBm input or 0.22 volts (rms) across the 50 ohm input impedance. To reach this signal level from the approximately 2.5 millivolt (rms) signal at the detector terminals requires a voltage gain of at least 88, or 39 dB. The i.f. amplifier is capable of providing 101 dB gain and has automatic gain control.

Figures 3-14 and 3-15 are schematic diagrams of the amplifier and discriminator.

3.6.4 Integrator

To convert the output signal from the FM discriminator into an analog of the phase of the i.f. signal (and hence, an analog of the modulation signal applied at the transmitter) requires the use of a broadband integrator. This is seen from the fact that the received signal voltage after conversion to the intermediate frequency ω_i, has the form

$$s(t) = A \sin \left|\omega_i t + \phi(t)\right| \qquad (3\text{-}1)$$

where $\phi(t)$ is the information term. The output of the FM discriminator will then be proportional to the instantaneous frequency of this signal which is given by

$$\omega = \omega_i + \frac{d\phi}{dt} \qquad (3\text{-}2)$$

The discriminator responds to the low frequency component of equation 3-2 which includes variations in the $\frac{d\phi}{dt}$ term occurring at rates below 2 MHz. The discriminator output was measured to be 1.5 volts per MHz of frequency deviation and its output signal, S_D, is therefore given by

$$S_D(t) = \frac{1.5 \times 10^{-6}}{2\pi} \frac{d\phi}{dt} \text{ volts} \qquad (3\text{-}3)$$

To convert the remaining information term to an analog of the modulation signal requires integration. This should be followed by amplification to achieve an output signal level of 0.5 V (peak). Assuming a sinusoidal modulation signal at $\omega_m = 2\pi$ (1 MHz) given by

$$\phi(t) = 0.22 \sin \omega_m t$$

gives

$$\frac{d\phi}{dt} = 0.22 \ (2 \times 10^6) \cos \omega_m t$$

and,

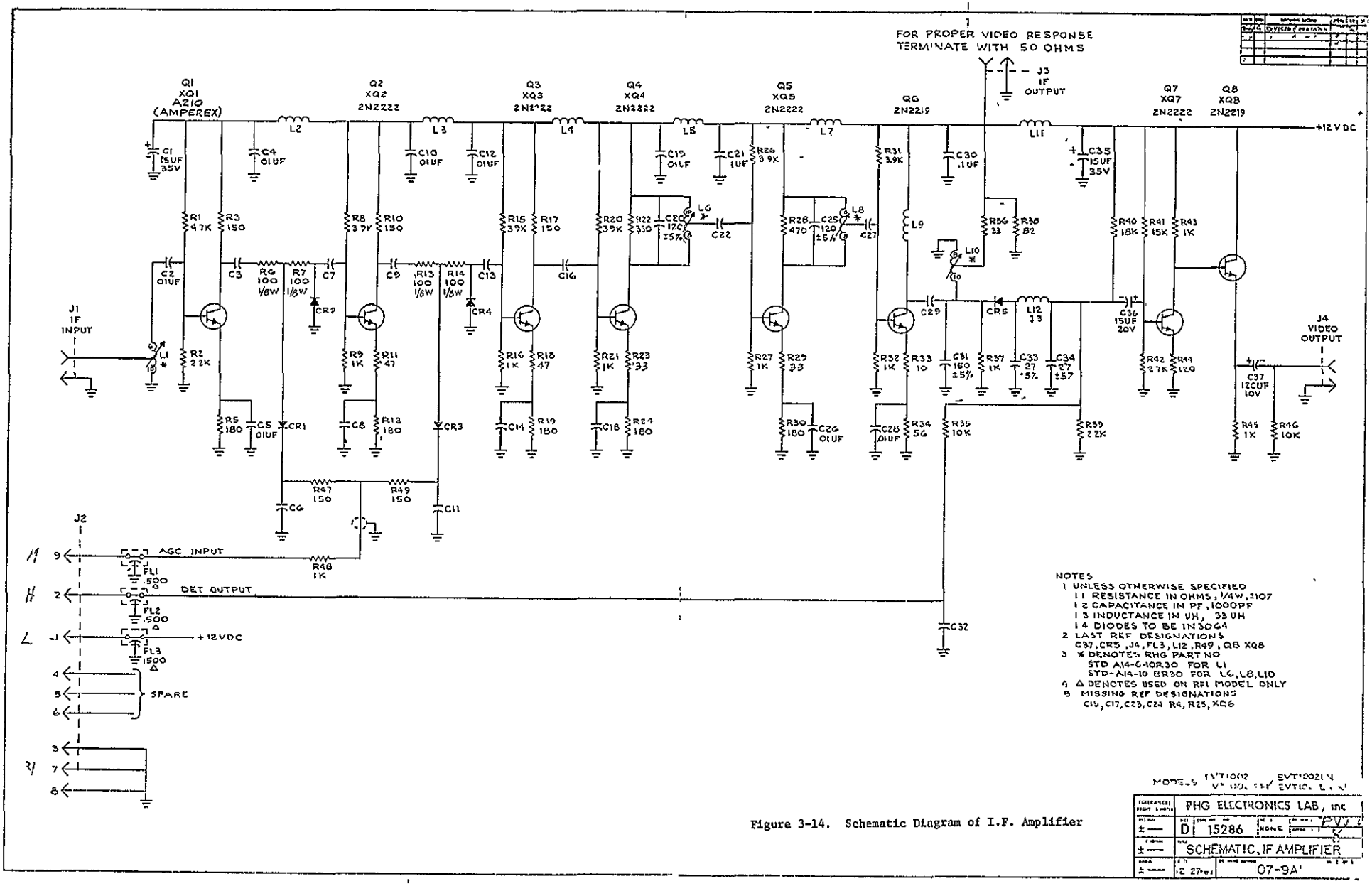

Figure 3-14. Schematic Diagram of I.F. Amplifier

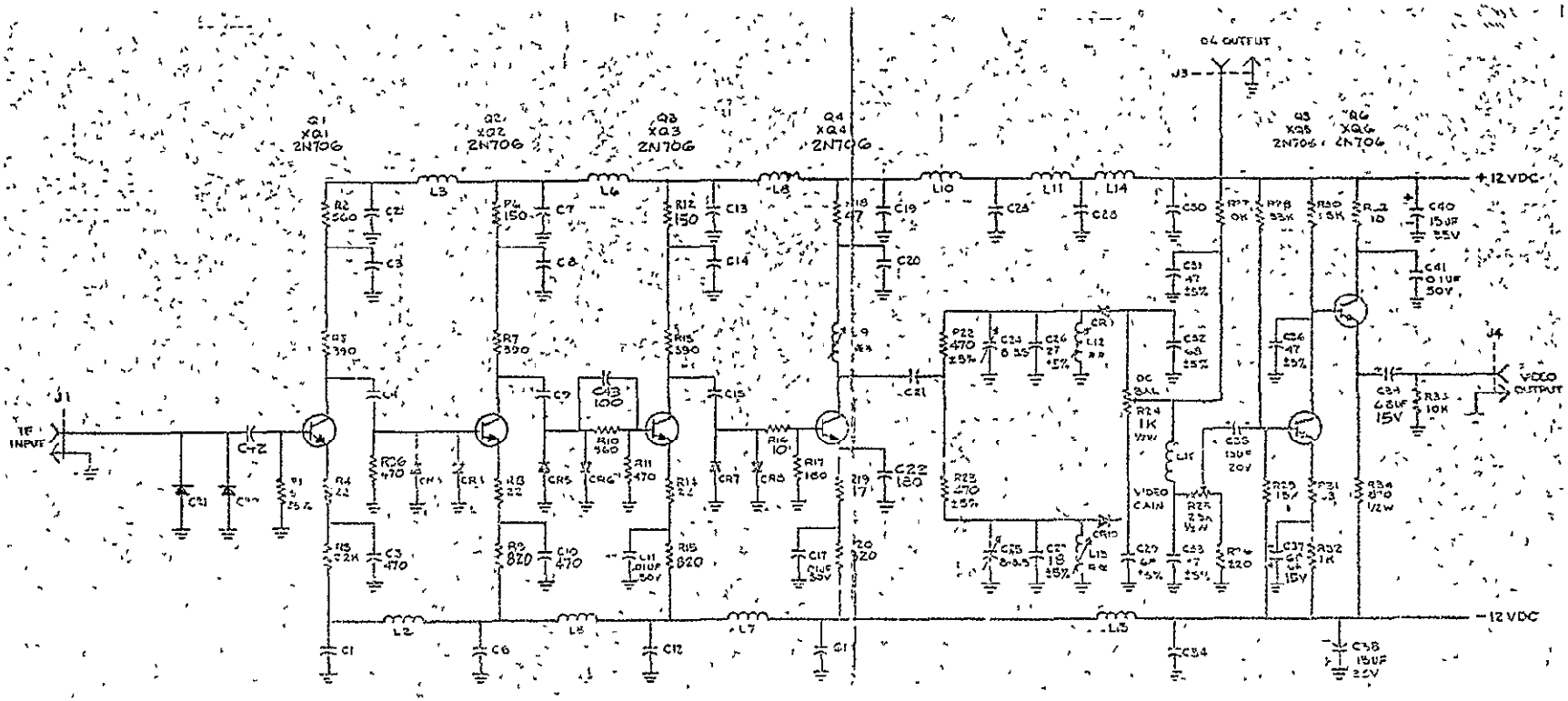

Notes

1. Unless otherwise specified·
   - 1.1 Resistance in ohms, 1/4W, ±10%.
   - 1.2 Capacitance in PF, 1000 PF..
   - 1.3 Inductance in UH, 240UH.
   - 1.4 Diodes to be 1N251.
2. Last Ref. Designations:
   C43, CR10; J4, L16, R36; Q6, XQ6.

Figure 3-15. Schematic Diagram of Limiter-Discriminator.

$$S_D(t)\Big|_{\omega_m = 1\ \text{MHz}} = 0.33 \cos \omega_m t$$

The gain of the integrator must, therefore, be about 1.5 at 1 MHz and must increase at the rate of 20 dB per decade at lower frequencies.

The circuit used to perform this function is shown in Figure 3-16.

Because of the large amount of low frequency noise due to laser frequency instability, the gain of this circuit was cut at low frequency to prevent gain saturation of the integrator. This was done by the use of capacitors in the input and output connections.

3.6.5 AFC Circuit

To accurately maintain the 10 MHz intermediate frequency between transmitter and local oscillator lasers required a feedback control loop which used the d.c. output of the FM discriminator as an error signal to control the frequency of the local oscillator laser. The control loop is a type 1 system which maintains the d.c. component of error at zero and reduces the a.c. fluctuations by the loop gain.

Figure 3-17 is a schematic diagram of the circuit which processes the error signal. This circuit uses a model D-9 operational amplifier made by Data Device Corporation. Loop gain and bandwidth characteristics for the AFC system are fixed by the R-C feedback network used with this amplifier.

The output of this circuit is then amplified by a high voltage amplifier and applied to the local oscillator piezoelectric cavity tuner to make the frequency corrections. This high voltage amplifier is a model 1000 ABC, 0 to 1000 volt programmable power supply made by Kepco Inc.. The dc gains for the elements in the elements used in the control loop are listed in Table 3-5.

REVISIONS				
ZONE	LTR	DESCRIPTION	DATE	APPROVED

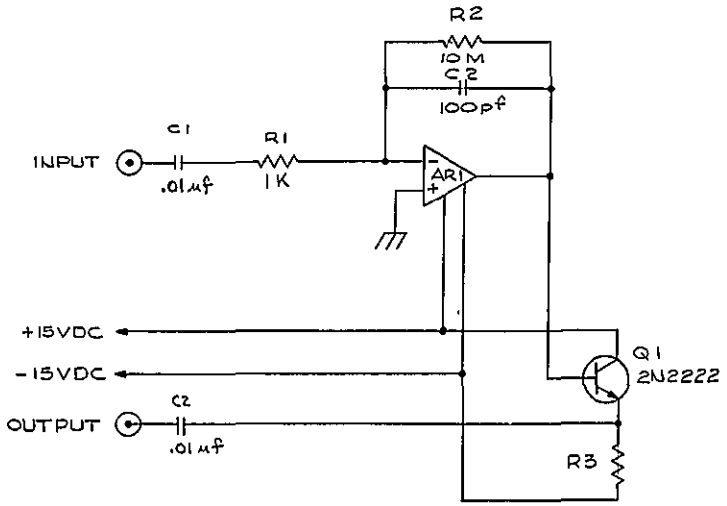

NOTES:
1 AR1 ZELTEX CORP TYPE 147M

QTY PER DASH NO	KEY	CODE IDENT	PART OR IDENTIFYING NO	SYLVANIA PART NO	NOMENCLATURE OR DESCRIPTION	NOTE	ITEM NO

PARTS LIST

KEY *—VENDOR ITEM—FOR PROCUREMENT OR PART NUMBER SEE SPECIFICATION CONTROL OR SOURCE CONTROL DRAWING
F—FEET I—INCHES B—BULK AR—AS REQUIRED

APPLICABLE DOCUMENTS	UNLESS OTHERWISE SPECIFIED DIMENSIONS ARE IN INCHES TOLERANCES ANGLES ± DECIMALS 2 PLACE ± 3 PLACE ± SURFACES √ MICRO INCHES	CONTRACT NO DR Ron Cole DATE 8/22/69 CHK APPD APPD RELEASE APPD BY	SYLVANIA ELECTRONIC SYSTEMS DIVISION OF SYLVANIA ELECTRIC PRODUCTS INC MOUNTAIN VIEW CALIFORNIA
FINISH	MATERIAL		A2 INTEGRATOR
NEXT ASSEMBLY / MODEL			SIZE C / CODE IDENT NO 07397 / DRAWING NO 478-0536 SCALE — SHEET 1 OF 1

Figure 3-16 Schematic Diagram of Integrator Circuit

SES-W 1755 (5-68)

REVISIONS				
ZONE	LTR	DESCRIPTION	DATE	APPROVED

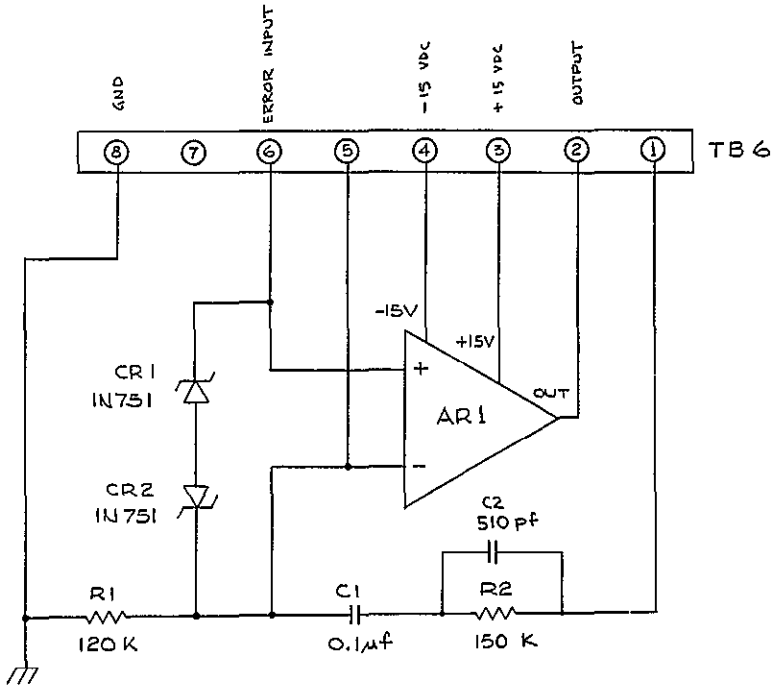

NOTES.

1. AR 1: DATA DEVICE CORP MODEL D9, OPERATIONAL AMPLIFIER

Figure 3-17 Schematic Diagram of AFC Amplifier Circuit

QTY PER DASH NO	KEY	CODE IDENT	PART OR IDENTIFYING NO	SYLVANIA PART NO	NOMENCLATURE OR DESCRIPTION	NOTE	ITEM NO

PARTS LIST

KEY X—VENDOR ITEM—FOR PROCUREMENT OR PART NUMBER SEE SPECIFICATION CONTROL OR SOURCE CONTROL DRAWING
F—FEET I—INCHES 8—BULK AR—AS REQUIRED

APPLICABLE DOCUMENTS	UNLESS OTHERWISE SPECIFIED DIMENSIONS ARE IN INCHES TOLERANCES ANGLES ± — DECIMALS 2 PLACE ± — 3 PLACE ± — SURFACES √ MICRO INCHES	CONTRACT NO DR Ken Cole DATE 8/12/69 CHK APPD APPD RELEASE APPD BY	SYLVANIA ELECTRONIC SYSTEMS DIVISION OF SYLVANIA ELECTRIC PRODUCTS INC MOUNTAIN VIEW CALIFORNIA
FINISH	MATERIAL		A1 LASER FREQUENCY CONTROL CIRCUIT
NEXT ASSEMBLY / MODEL			SIZE C · CODE IDENT NO 07397 · DRAWING NO 478-0534 SCALE — · SHEET 1 OF 1

SES-W 1755 (5-68)

Table 3-5

D.C. Gain of Elements in AFC Loop

FM discriminator	0.16 V/MHz
AFC amplifier circuit	10^4
Kepco amplifier	27
Piezoelectric Transducer	1.5 MHz/volt
Total dc loop gain	6.5×10^4

Gain for the control loop drops to unity at approximately 100 Hz.

3.7 Transmitter System

The transmitter system consists of an assembly containing the laser, modulator, and transmitting telescope and a separate control console containing power supplies and control functions for the laser and modulator. Figure 3-18 is a photograph of the transmitter, showing the location of principal components, including the laser, modulator, and telescope. Covers have been removed from the laser and modulator for this photograph.

Figure 3-19 is a photograph of the control console, showing the principal components. The laser power supplies are model 10030 AM regulated high voltage power supplies made by Northeast Scientific Corp. Specifications for the supplies are shown in Table 3-6.

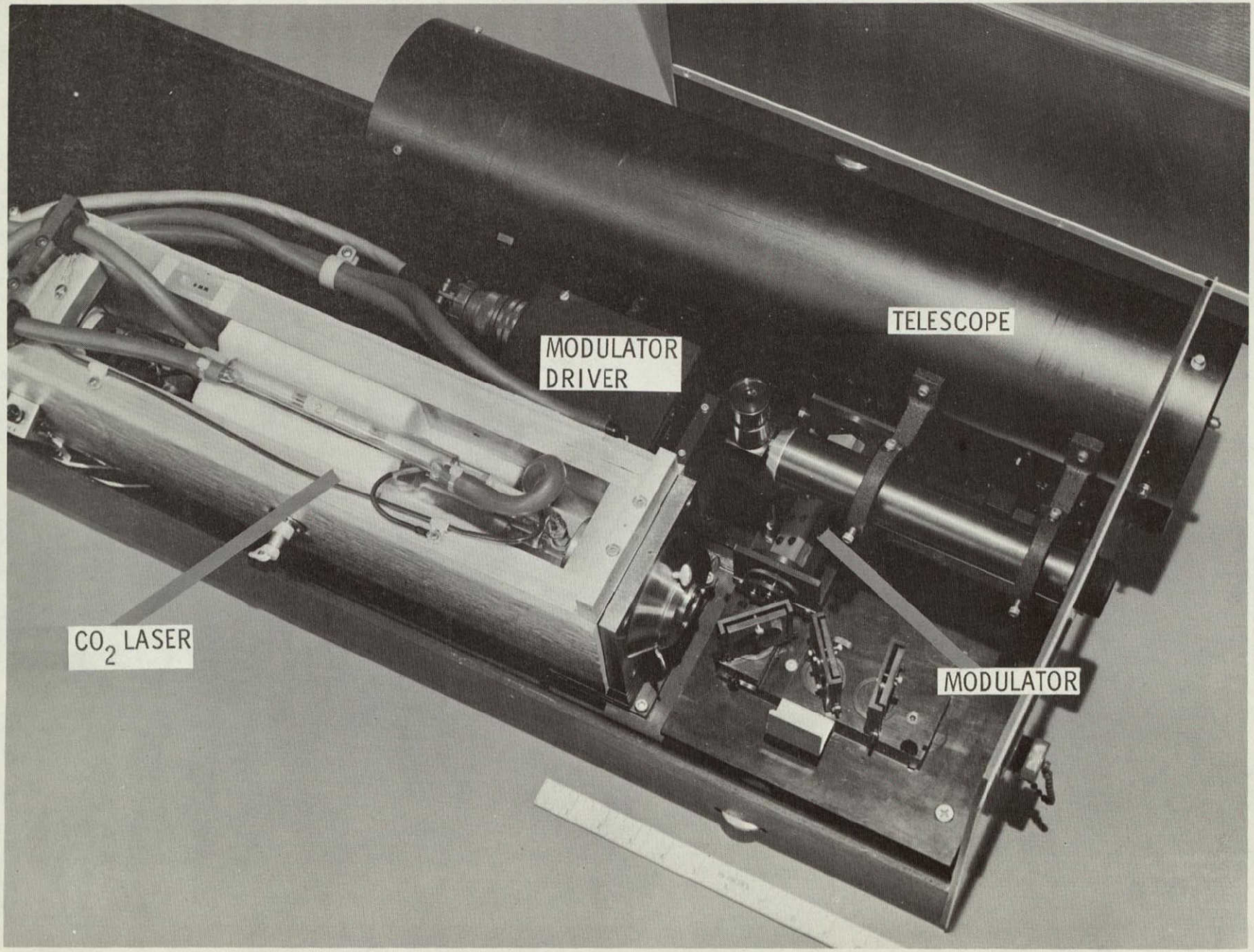

Figure 3-18. Photograph of 10.6 Micron Transmitter.

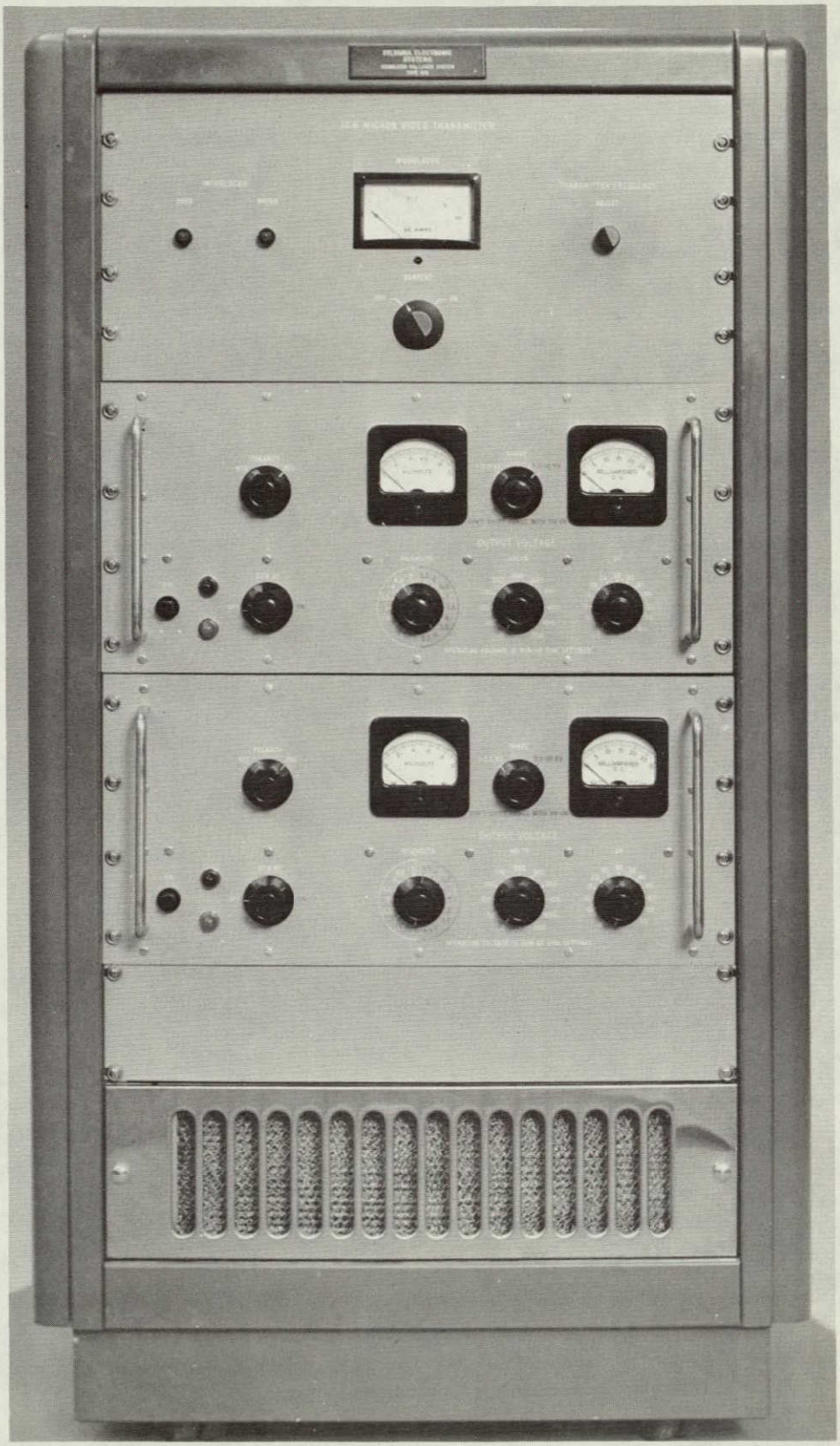

Figure 3-19. Transmitter Control Console.

Table 3-6

Plasma Power Supply Specifications

Output Voltage:	1 to 10 kV DC
Output Current:	0 to 30 mA
Ripple:	less than 5 mV p-p
Output Regulation:	.002% no load to full load
Stability:	.01% for line voltage shift between 105 V and 125 V
Power Input:	550 watts max.

Only one of the high voltage power supply is used; the second power supply functions as a spare unit. (It was originally used to operate a CO_2 amplifier tube for laser stabilization studies.)

Interlock switches are provided which prevent operation of the transmitter unless cooling water is flowing and the rear door to the console is closed. In normal use, power for the transmitter is controlled from the on-off switch on the high voltage power supply. This switch controls power for all functions except for the laser cavity temperature controller, which remains turned on when the lasers are not in use. For extended storage periods, all power to the transmitter system can be switched off with the circuit breaker inside the rear door of the control console. Other front panel controls include:

1) modulator on-off
2) laser frequency control
3) laser plasma current adjust.

Figure 3-20 is an electrical interconnection diagram for the transmitter system.

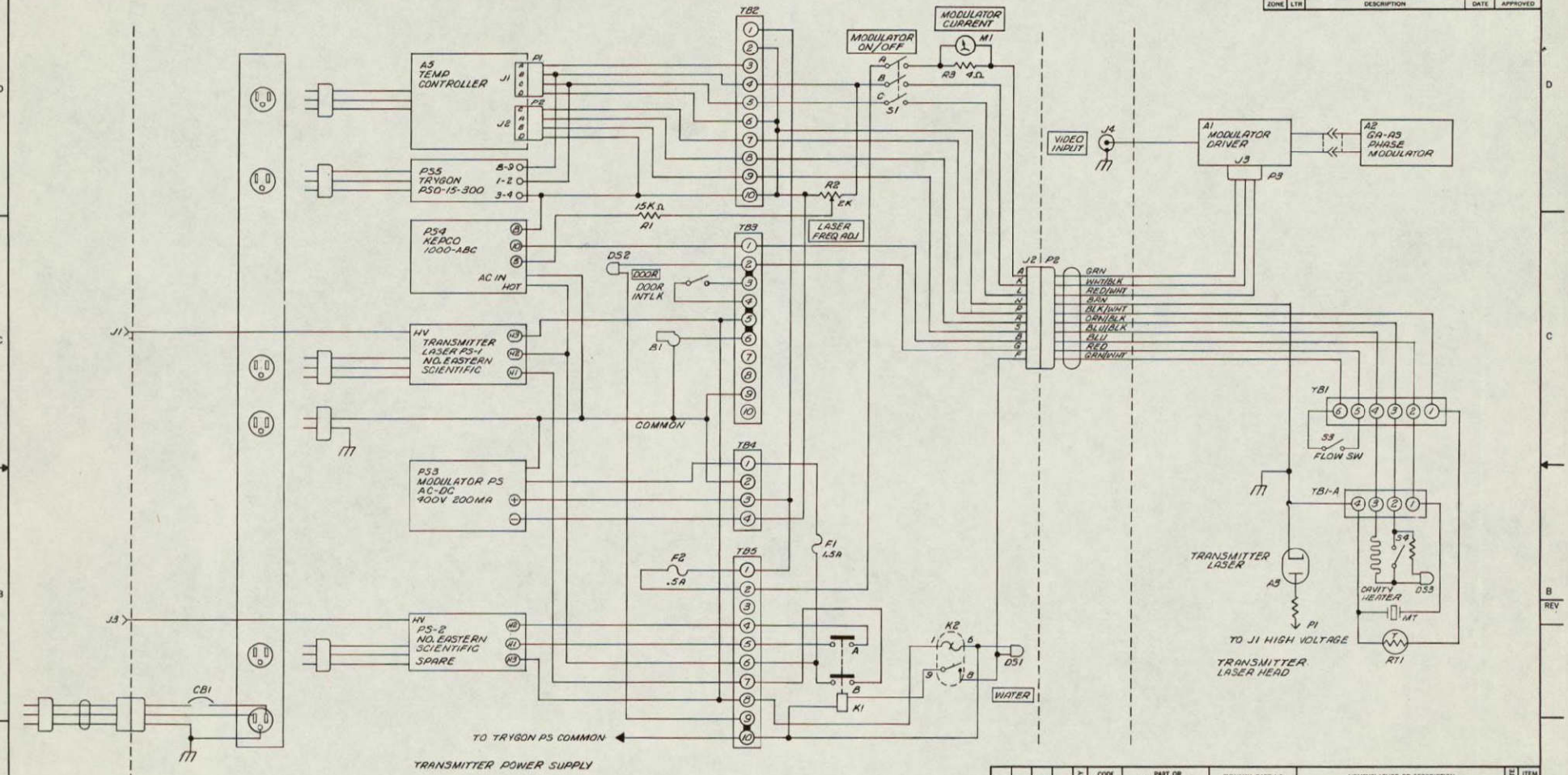

Figure 3-20. Transmitter Electrical Interconnection Diagram.

REVISIONS

ZONE	LTR	DESCRIPTION	DATE	APPROVED

PARTS LIST

KEY: V—VENDOR ITEM—FOR PROCUREMENT OR PART NUMBER SEE SPECIFICATION CONTROL OR SOURCE CONTROL DRAWING
F—FEET I—INCHES B—BULK AR—AS REQUIRED

QTY PER DASH NO.	KEY	CODE IDENT	PART OR IDENTIFYING NO.	SYLVANIA PART NO.	NOMENCLATURE OR DESCRIPTION	NOTE	ITEM NO.

APPLICABLE DOCUMENTS

UNLESS OTHERWISE SPECIFIED DIMENSIONS ARE IN INCHES
TOLERANCES
ANGLES ± —
DECIMALS
2 PLACE ± —
3 PLACE ± —
SURFACES MICRO-INCHES

FINISH

MATERIAL

NEXT ASSEMBLY | MODEL

DR G.W.Smith DATE 5 SEP 65
CHK
APPD
APPD

SYLVANIA ELECTRONIC SYSTEMS
DIVISION OF SYLVANIA ELECTRIC PRODUCTS INC
MOUNTAIN VIEW, CALIFORNIA

INTERCONNECTION DIAGRAM - TRANSMITTER

SIZE D | CODE IDENT 07397 | 478-0533

SCALE — | SHEET / OF /

SES-W-1756 (6-65)

3.8 Receiver System

The receiver system consists of separate receiver and control console units similar to the transmitter system. Figure 3-21 is a photograph of the receiver unit showing the location of the major components.

The control console for the receiver is similar to the transmitter control console in that the same laser power supplies are used. Figure 3-22 is a photograph of the console, showing the various front panel functions and controls including:

1) receiver on-off
2) laser frequency control
   a) manual
   b) AFC
   c) external
3) laser current control
4) laser power meter
5) AFC error meter

In addition to having the same type of interlocks as the transmitter system, the receiver system has an additional interlock which interrupts both electrical and optical power to the Ge:Au detector when there is no liquid nitrogen in the dewar. In normal operation, when the liquid nitrogen level gets low, an audible warning sounds approximately 20 minutes before this interlock is actuated, indicating that the dewar should be re-filled.

Figure 3-23 shows the electrical interconnections for the receiver system

Figure 3-24 is a photograph of the complete communication system, including both the transmitter and receiver system.

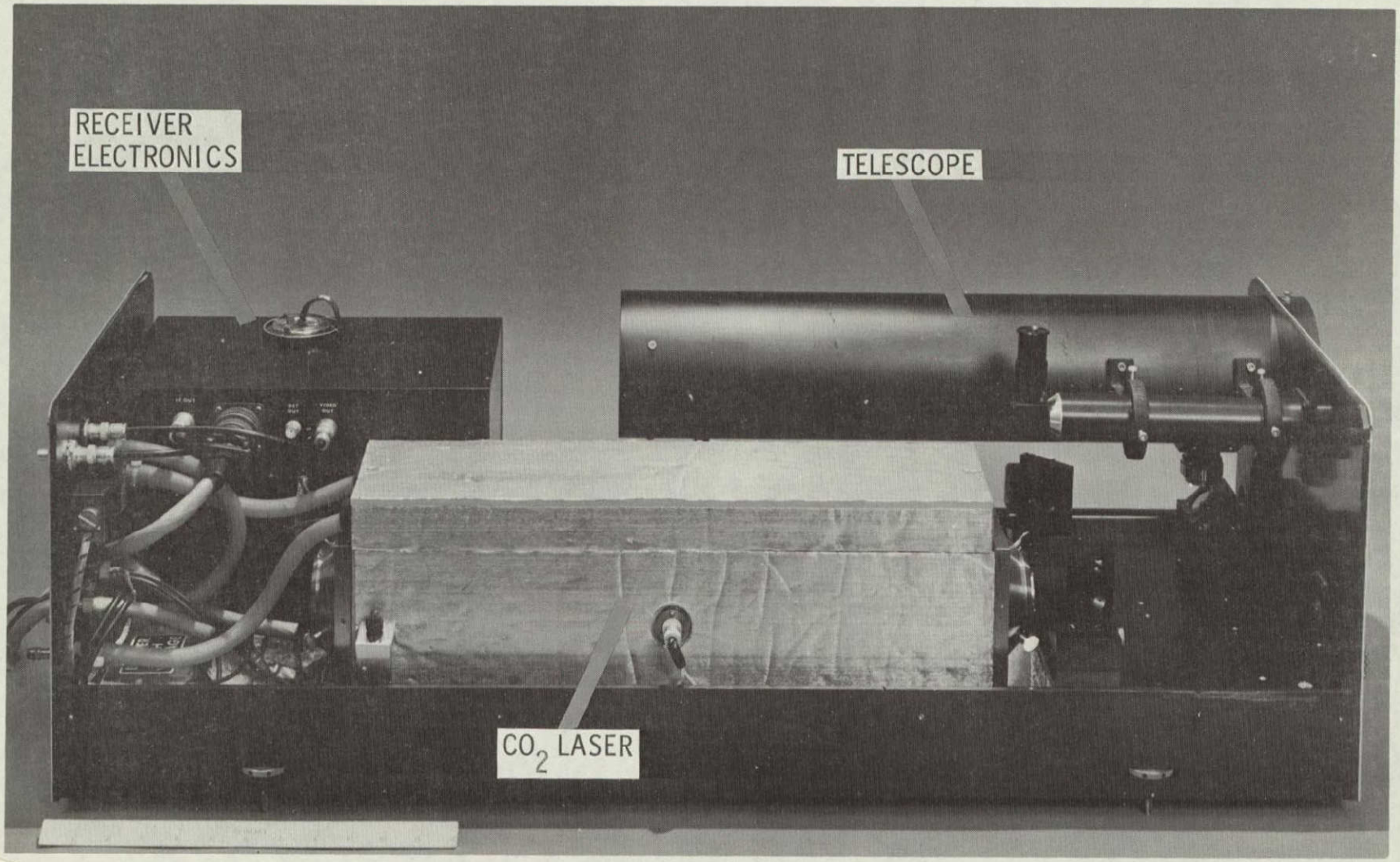

Figure 3-21. Photograph of 10.6 Micron Receiver.

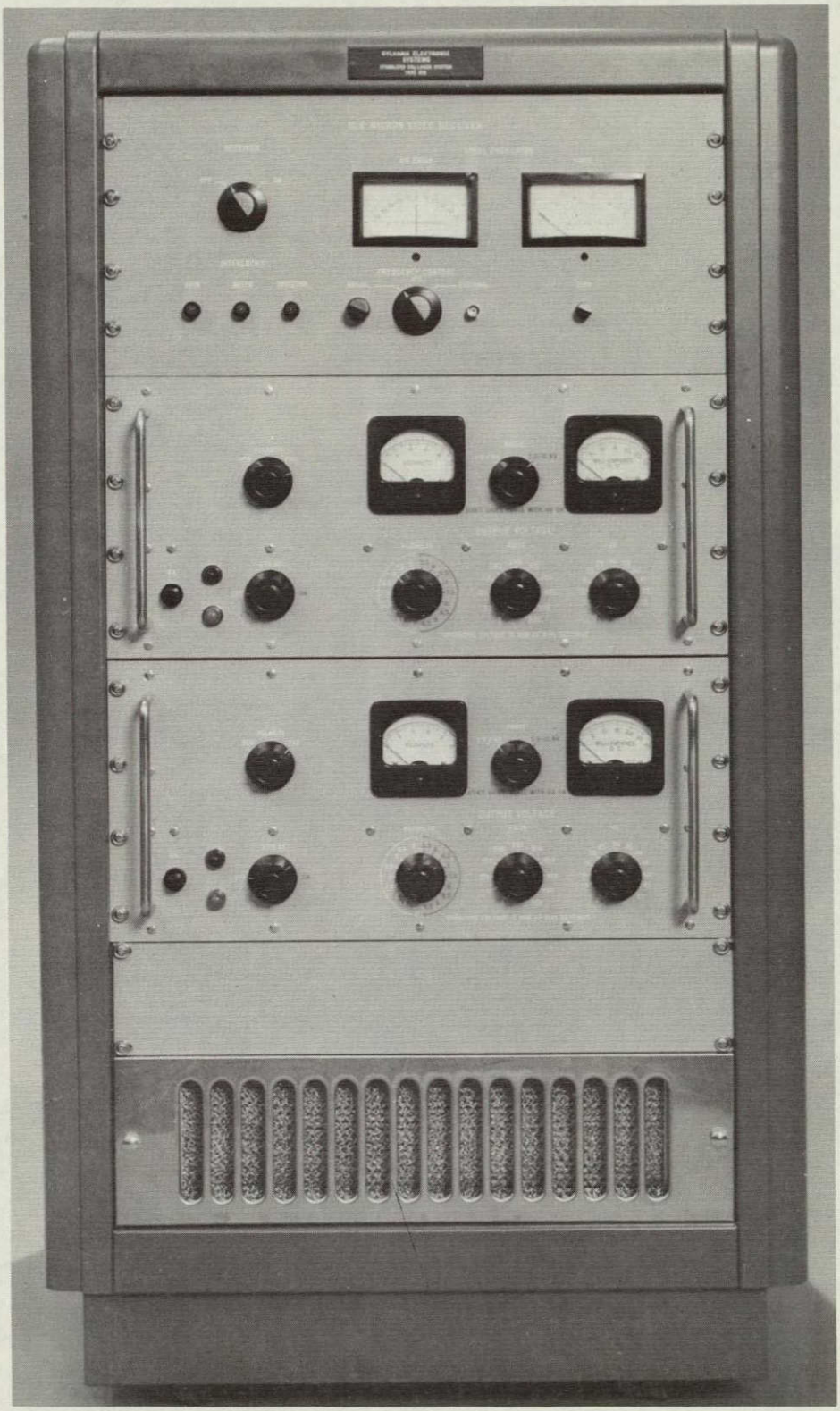

Figure 3-22. Receiver Control Console.

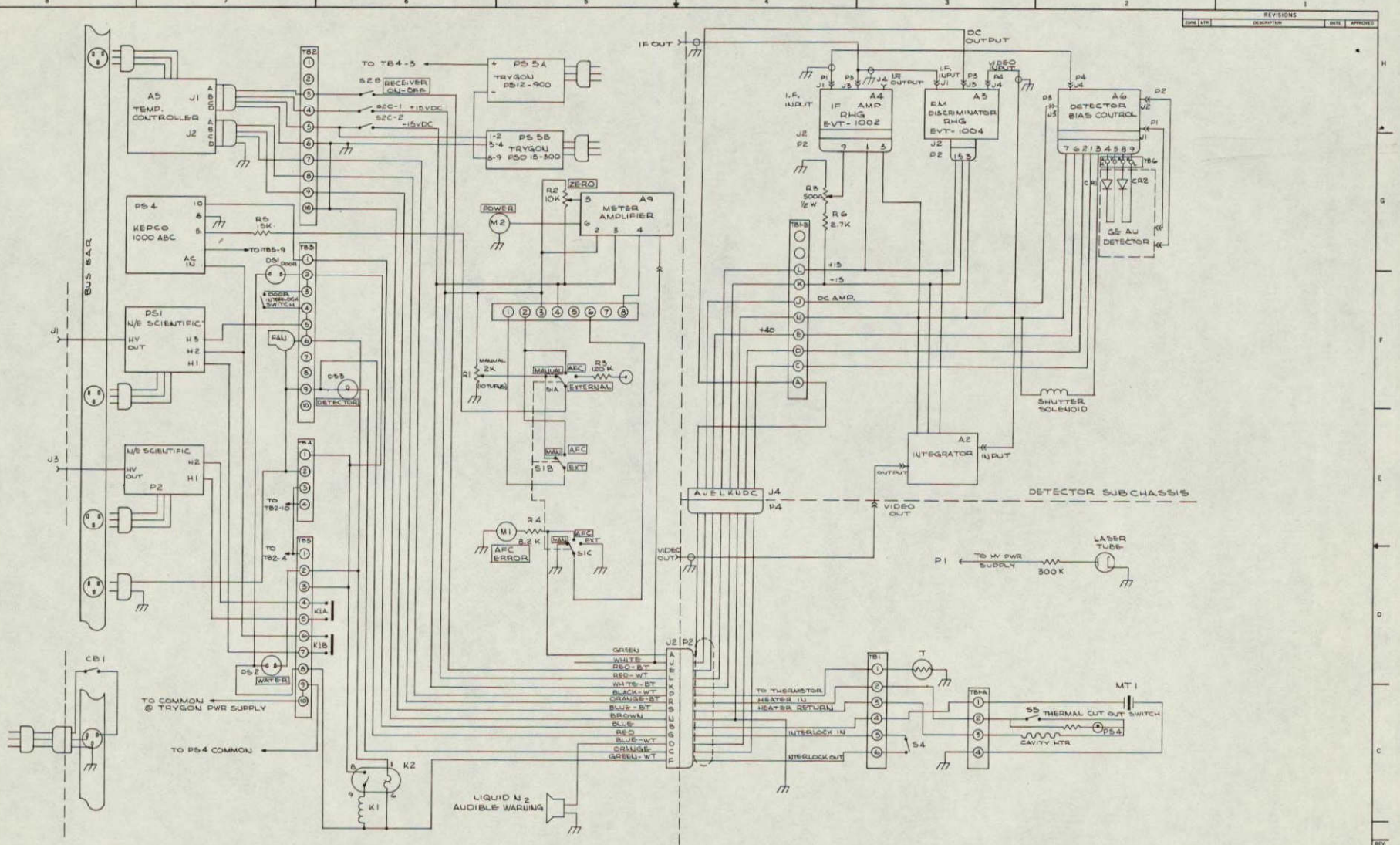

Figure 3-13. Receiver Electrical Interconnection Diagram.

PARTS LIST					
QTY PER DASH NO.	CODE IDENT	PART OR IDENTIFYING NO.	SYLVANIA PART NO.	NOMENCLATURE OR DESCRIPTION	REF NO.

KEY: A—VENDOR ITEM—FOR PROCUREMENT OR PART NUMBER SEE SPECIFICATION CONTROL OR SOURCE CONTROL DRAWING
F—FEET I—INCHES B—BULK AR—AS REQUIRED

APPLICABLE DOCUMENTS	UNLESS OTHERWISE SPECIFIED DIMENSIONS ARE IN INCHES TOLERANCES ANGLES ± DECIMALS 2 PLACE ± 3 PLACE ±	DR. J. Cole CHK APPD APPD	SYLVANIA ELECTRONIC SYSTEMS DIVISION OF SYLVANIA ELECTRIC PRODUCTS INC MOUNTAIN VIEW, CALIFORNIA
FINISH NEXT ASSEMBLY / MODEL	MATERIAL		INTERCONNECTION DIAGRAM - RECEIVER SIZE E · CODE IDENT 07397 · 478-0532 SCALE · SHEET 1 OF 1

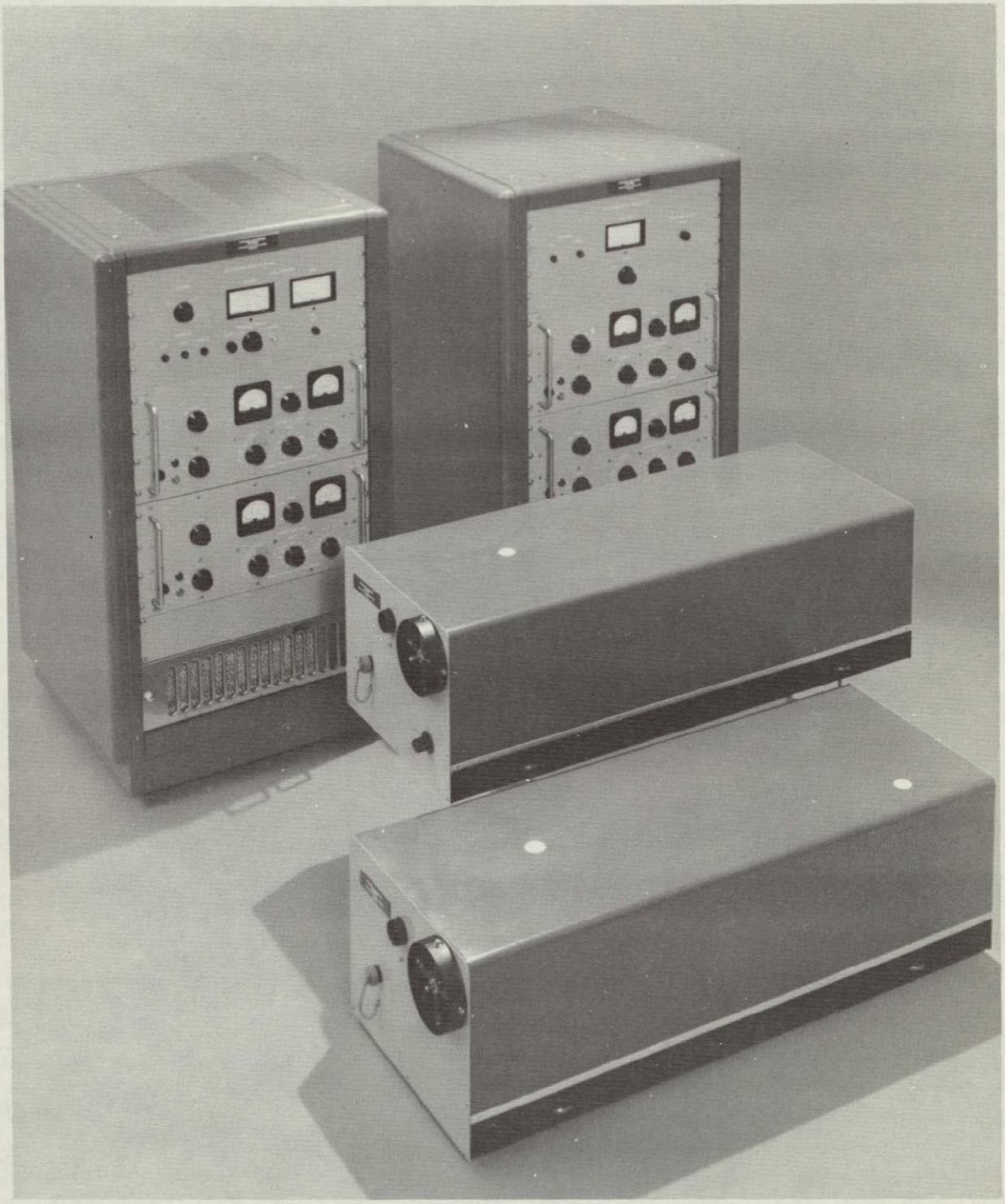

Figure 3-24. 10.6 Micron Communication System.

SECTION 4.0

SYSTEM PERFORMANCE

4.1 Introduction

After construction and assembly of the components described in Section 3, the transmitter and receiver were set up and aligned for testing over a short indoor propagation path. Separation between the transmitter and receiver was approximately 3 meters, which resulted in essentially no losses due to atmospheric absorption or diffraction. This allowed measurements of transmission efficiency for the system to be made independent of these effects. The arrangement also allowed measurements of signal and noise performance to be made independent of long atmospheric path effects.

4.2 Optical Power Flow

The following table summarizes the 10.59 micron optical power levels measured at several locations in the transmitter.

Table 4-1

Optical Power Levels in Transmitter at 10.59 Microns

Laser Output	1.1 watts
Power through First Beamsplitter	110 mW
Power at Modulator Output	400 mW

With 400 mW input to the transmitter telescope, the power level at the output of the receiver telescope was 150 mW. This is approximately half the value expected at this point based on the expected transmission efficiencies of the two telescopes. It is, however, not too surprising since accurate alignment of the two telescopes is made difficult by inability to form a visible image of the beam. It is quite possible that the two telescopes were not perfectly aligned and that some part of the transmitted beam was not being collected by the receiver telescope.

Another significant loss may have been incurred if the shadow of the diagonal mirror in the telescope was not perfectly aligned with the diagonal mirror in the receiver scope. In the receiver, the following power levels were measured.

Table 4-2
Optical Power Levels in Receiver at 10.59 Microns

Local Oscillator Laser Output	700 mW
Power Transmitted through First Beamsplitter	75 mW
L.O. Power at Detector	280 mW
Signal Power at Detector	70 mW

With the relatively large amount of signal power available at the detector, very little difficulty was encountered in obtaining a heterodyne beat note between the lasers. This allowed the various electronic subsystems including the receiver and modulator electronics to be checked out easily.

4.3 Receiver Electronics Performance

Before the communication channel can be used, proper operation of the automatic frequency control function is necessary in order to keep the laser heterodyne beat frequency within the relatively narrow passband of the i.f. amplifier. The AFC performed very well during tests with the system. To acquire the 10 MHz i.f., the following procedure was used: The transmitter laser was tuned in frequency for maximum power output. This insured that it was operating near the center of the 10.59 micron transition. The local oscillator was then manually tuned in frequency until a deflection of the AFC error meter was observed. Moving the L.O. frequency control switch from manual control to the AFC position resulted in immediate stabilization of the i.f.. Figure 4-1 shows a time recording

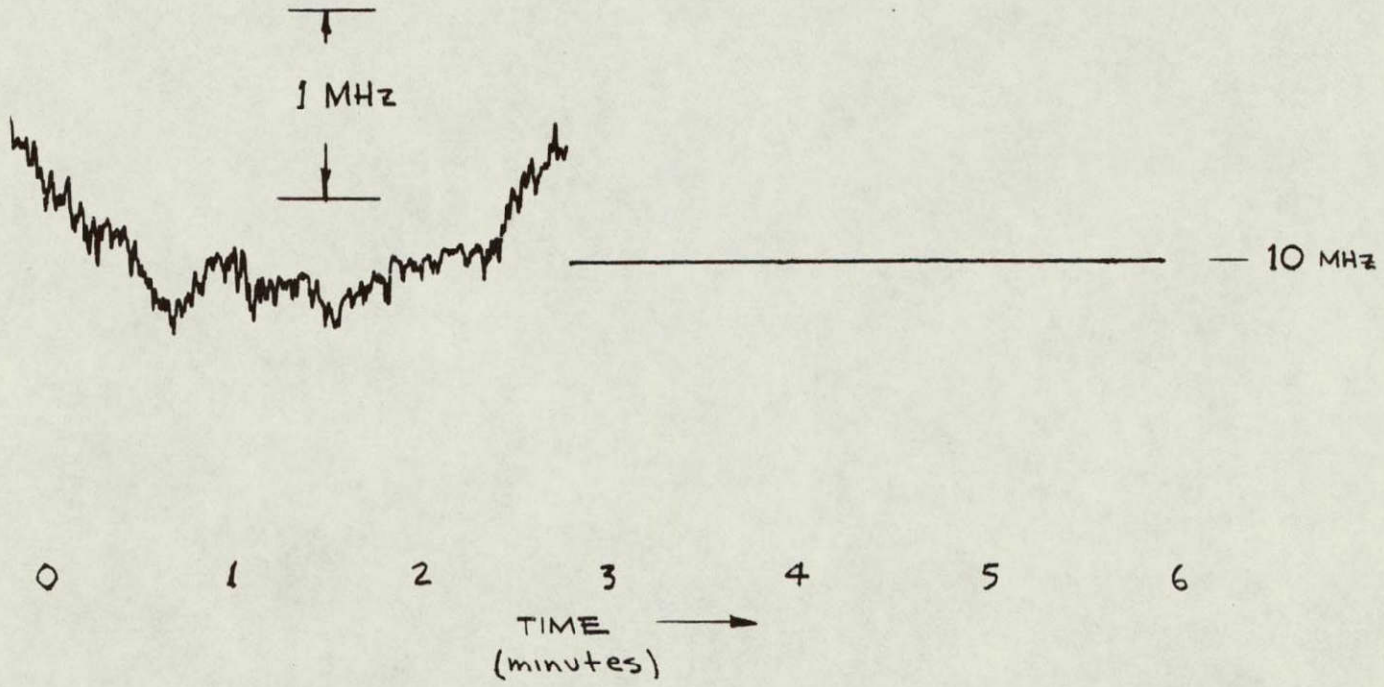

Figure 4-1. Heterodyne Beat Frequency Before and After Activation of AFC.

of the beat frequency before and after activation of the AFC function.

Display of the i.f. signal on a spectrum analyzer showed that the characteristic width of the heterodyne signal is about 6 kHz for observation periods on the order of a millisecond. For longer observation periods, the signal was observed to drift back and forth within a range of about ±10 kHz when the lasers were locked by the AFC loop. Figure 4-2 shows photographs of the spectrum analyzer display for two different observation intervals.

The fluctuations observed in the intermediate frequency produced a noise signal at the output of the FM discriminator having an rms level of a few millivolts. Also contained in the discriminator output signal were significant components at harmonics of the 60 Hz power line frequency which were picked up and fed to the FM discriminator through its power supply leads. This effect was reduced by more than an order of magnitude from its origianl level, but could not be eliminated.

Noise occurring at higher frequencies near 400, 1000 and 1600 Hz was presumably due to acoustic noise in the room produced by the power supply cooling fans and other sources. The noise occurring near 1600 Hz appears to be due to a mechanical resonance associated with the laser cavity structure.

When the discriminator signal was fed to the integrator, the large low frequency gain resulted in a noise output voltage from the receiver of approximately 20 volts. It was therefore necessary to reduce the low frequency gain of the integrator, thereby reducing the low frequency response of the communication channel. This kept the signal output at higher frequencies from being obscured by the low frequency noise. Figure 4-3 shows the spectral characteristics of this noise output from the receiver.

The performance of the communication system is characterized by the plot shown in Figure 4-4, showing the amplitude of the signal at the

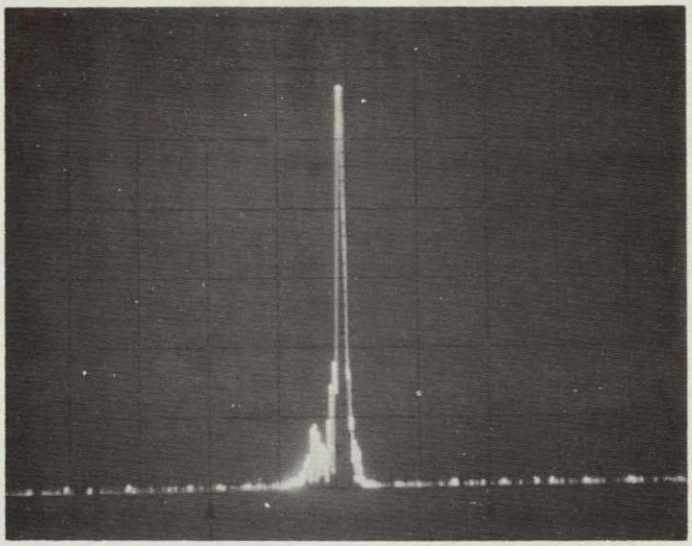

30 KHz / DIV
SINGLE SWEEP AT 3 m sec. / DIV

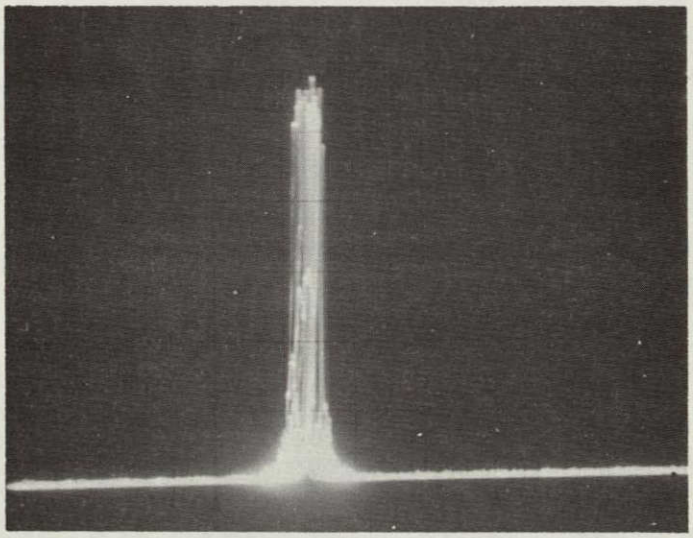

30 KHz / DIV
1 SEC EXPOSURE

Figure 4-2. Spectrum Analyzer Display of Heterodyne Beat Signal for Two Different Observation Periods.

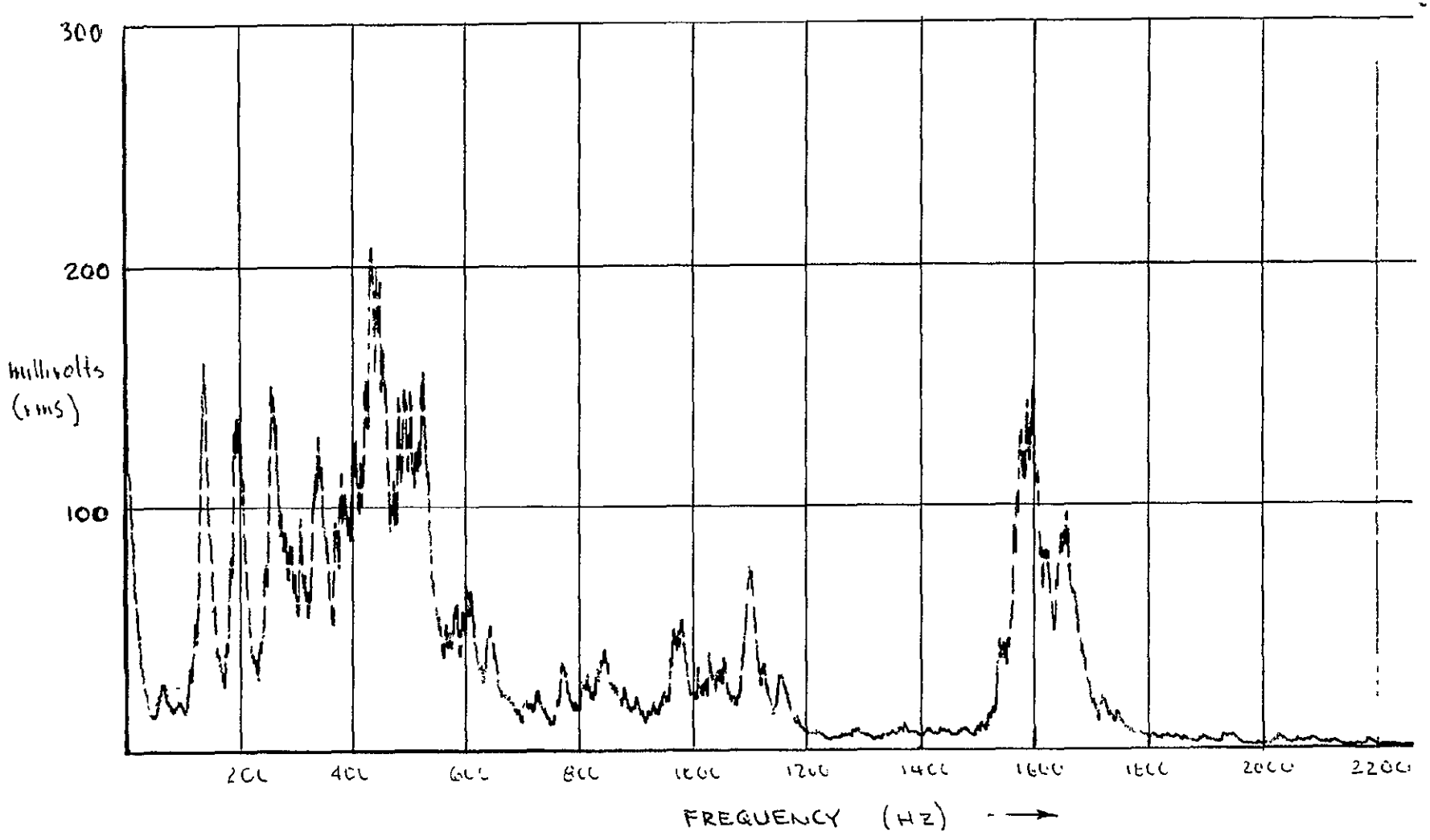

Figure 4-3. Spectrum Analysis of Receiver Low Frequency Noise Output.

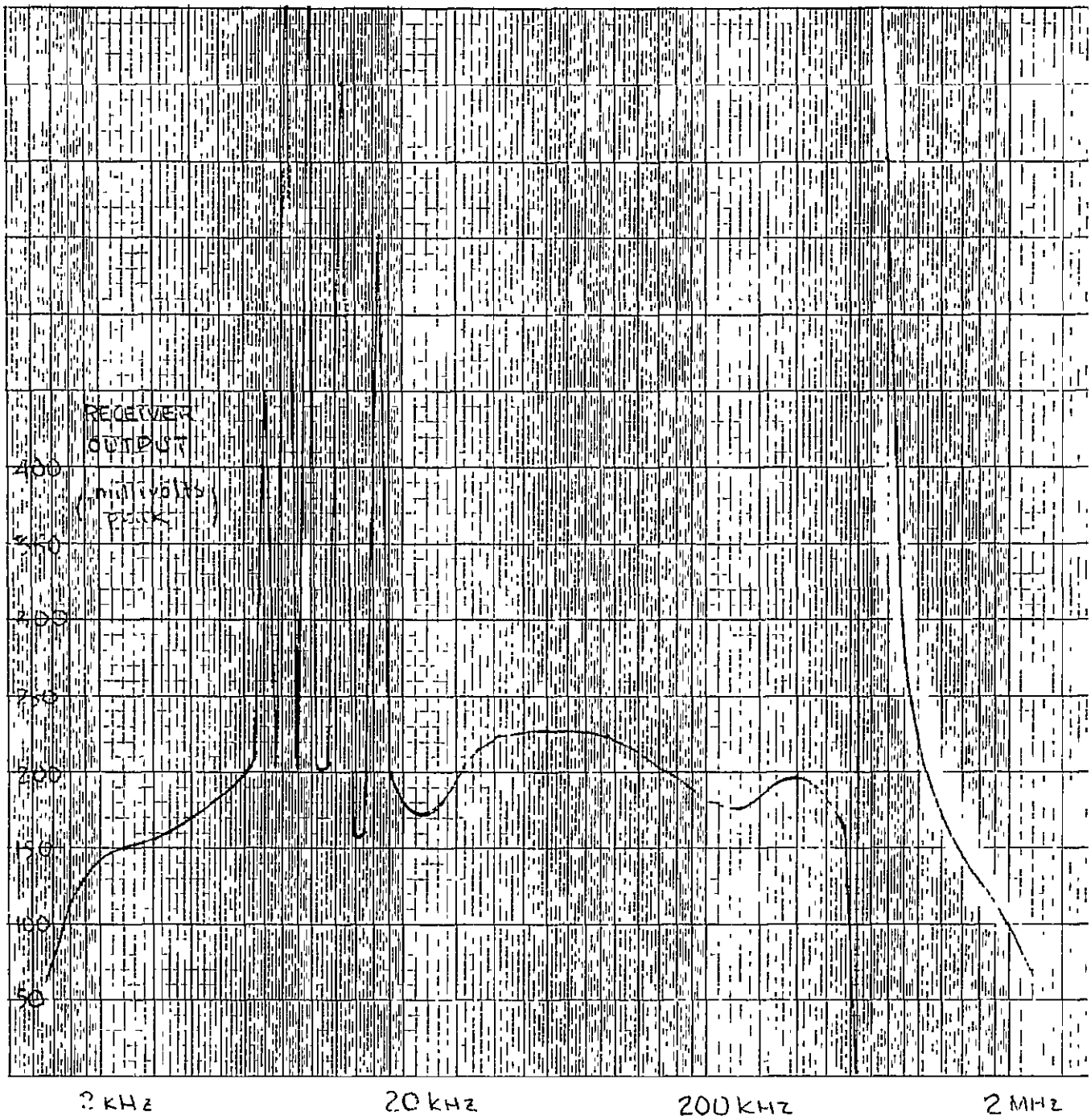

Figure 4-4. Receiver Output Amplitude vs. Frequency for 0.5 V (peak) Signal Input at Transmitter.

receiver output produced by a constant amplitude (0.5 V) signal input at the transmitter. Notable features in the data include the multiple peaks occurring between 7 and 17 kHz. The origin of this effect is apparently in the modulator, since none of the receiver electronics components demonstrated such resonances in prior tests. The exact cause is not known, but it is conceivable that the electrical force produced by Coulomb attraction between the modulator electrodes is exciting mechanical resonances in the modulator holder. The other important effect is the fundamental modulator resonance which occurs at 690 kHz.

These effects, plus the fact that the vertical synchronization pulses for the television monitor occur at a rate below the low frequency cutoff for the system prevented satisfactory transmission of television pictures.

The most fundamental limitation on bandwidth for the phase modulation system is the low frequency noise problem. This problem can, however, be solved by converting the system for AM transmission as described previously in Section 3.4. Reduction of the modulator resonance effects will be a matter of careful attention to clamping of the modulator rods and the design of the modulator rod holder to eliminate mechanical resonances.

Another possibility for skirting the problem of modulator resonances is to use frequency conversion techniques to convert the information band from baseband up to, say, the band between 1 and 3 MHz. In this way the modulator is driven at frequencies above those which produce the problem.

SECTION 5.0

CONCLUSIONS AND RECOMMENDATIONS

The communication system which has been constructed demonstrates the feasibility of a rugged, relatively compact and simple to operate CO_2 laser heterodyne system. Long-life sealed-off CO_2 laser oscillators having excellent stability characteristics while remaining compact, rugged and lightweight are employed. During tests, these lasers have performed in a manner qualifying them as relaible components which, unlike previous counterparts, do not require continual care and attention.

The modulation technique used in the present implementation was phase modulation by means of the electro-optic effect in GaAs. A broadband high-voltage transistor amplifier was developed for use with the modulator, demonstrating the feasibility of driving this type of modulator with a very compact and reliable source which uses state-of-the-art solid state circuit design techniques. Power required by the driver to produce 0.22 radians peak phase modulation depth over the 2 MHz bandwidth was approximately 65 watts. Further substantial reduction in power drain can be obtained by employing complementary transistor pairs in the present balanced drive configuration.

The broadband phase modulation technique allowed examination of electro-optic modulator resonance problems and the techniques for suppressing them. Further development work on GaAs electro-optic modulators appears necessary to eliminate these problems. Clamping the modulator rods not only between lead electrodes (as was done in the present system) but also between acoustically lossy dielectric material on the sides will further reduce the resonance effect. Further reduction of the 690 kHz resonance can be obtained by use of an electronic "notch" filter tuned to that frequency following the i.f. amplifier. Another technique which can be used to completely avoid the resonance problem is to simply convert the baseband information up to a band which does not include the resonance, and then down-convert again at the receiver.

The modulation technique used with this system also allowed critical evaluation of the noise performance of a CO_2 laser phase modulation system. It must be concluded that sufficient phase stability between the laser oscillators at low audio rates for reception of information at frequencies below 2 to 5 kHz is not easily obtainable. A relatively minor modification to the present system would extend the useable bandwidth of the system to lower frequencies and improve the signal-to-noise performance: By inserting a $\lambda/4$ wave-plate in front of the modulator, it will be possible to convert to an amplitude modulation system, eliminating the low frequency noise problem caused by oscillator phase noise. An AM modulation depth of about 20% is feasible with the present modulator and modulator driver.

Additional features which could be added to increase the utility of the system include the following:

1) A temperature-insensitive etalon wavelength-identifier in the transmitter test output. Such an etalon can be readily fabricated from two reflectors separated by a very thin air gap.

2) A visible alignment laser in the transmitter, whose beam is combined and collimated with the 10.6 micron beam after it has passed through the modulator and prior to entering the telescope.

3) A photodetector and receiver electronics for use at the transmitter test output for evaluation of modulator performance. This would be used when the laser receiver system is at a remote site.

In conclusion, the present system represents a transition in the development of the CO_2 laser and laser related components from laboratory research instruments to useful field hardware capable of reliable performance. With modifications to this system, it can be adapted for specific application in terrestrial and/or airborne 10.6 micron communications experiments.

SECTION 6.0

REFERENCES

Section 1.0

1-1 A. E. Siegman, "Absolute Frequency Stabilization of a Laser Oscillator Against a Laser Amplifier", IEEE Jour. Quantum Electronics, QE-3, pp 337-339, July 1967.

1-2 R. S. Reynolds, A. E. Siegman, J. D. Foster, R. Rogers, "Frequency-Stabilized CO_2 Lasers", Phase One Report, Contract NAS 8-20631, 12 August 1966.

1-3 M. W. Sasnett, R. S. Reynolds, "Frequency-Stabilized CO_2 Lasers", Phases Three and Four Report, Contract NAS 8-20631, 1 October 1969.

Section 2.0

2-1 I. P. Kaminow, "Measurements of the Electrooptic Effect in CdS, ZnTe and GaAs at 10.6 Microns", IEEE Jour. Quant. Electronics, QE-4, pp 23-26, January 1968.

2-2 These values were calculated from data supplied by the manufacturer of this detector; Santa Barbara Research Center, Goleta, California.

2-3 J. C. Stephenson et al. "Atmospheric Absorption of CO_2 Laser Radiation" App. Phys. Lett., 11, 164-166, 1 Sept. 1967.

Section 3.0

3-1 T. J. Bridges, H. A. Haus, P. W. Hoff, "Small-Signal Step Response of Laser Amplifiers and Measurement of CO_2 Laser Linewidth", IEEE Jour. of Quantum Electronics, Vol. QE-4, pp 777-782, November 1968.

3-2 M. W. Sasnett, R. S. Reynolds, P. J. Titterton, A. E. Siegman, "10.6 Micron Laser Freqency Control Techniques", Technical Report AFAL-TR-68-210, September 1968.

3-3 S. Namba, "Electro-Optical Effect of Zincblende", Jour. Opt. Soc. of Am., Vol. 51, pp 76-79, January 1961.

3-4 F. Sterzer, D. Blattner, S. Miniter, "Cuprous Chloride Light Modulators", Jour Opt. Soc. of Am., Vol. 54, pp 62-68, January 1964.

3-5 I. P. Kaminow, "Measurements of the Electrooptic Effect in CdS, ZnTe, and GaAs at 10.6 Microns", Jour. Quantum Electronics, Vol. QE-4, pp. 23-26, January 1968.

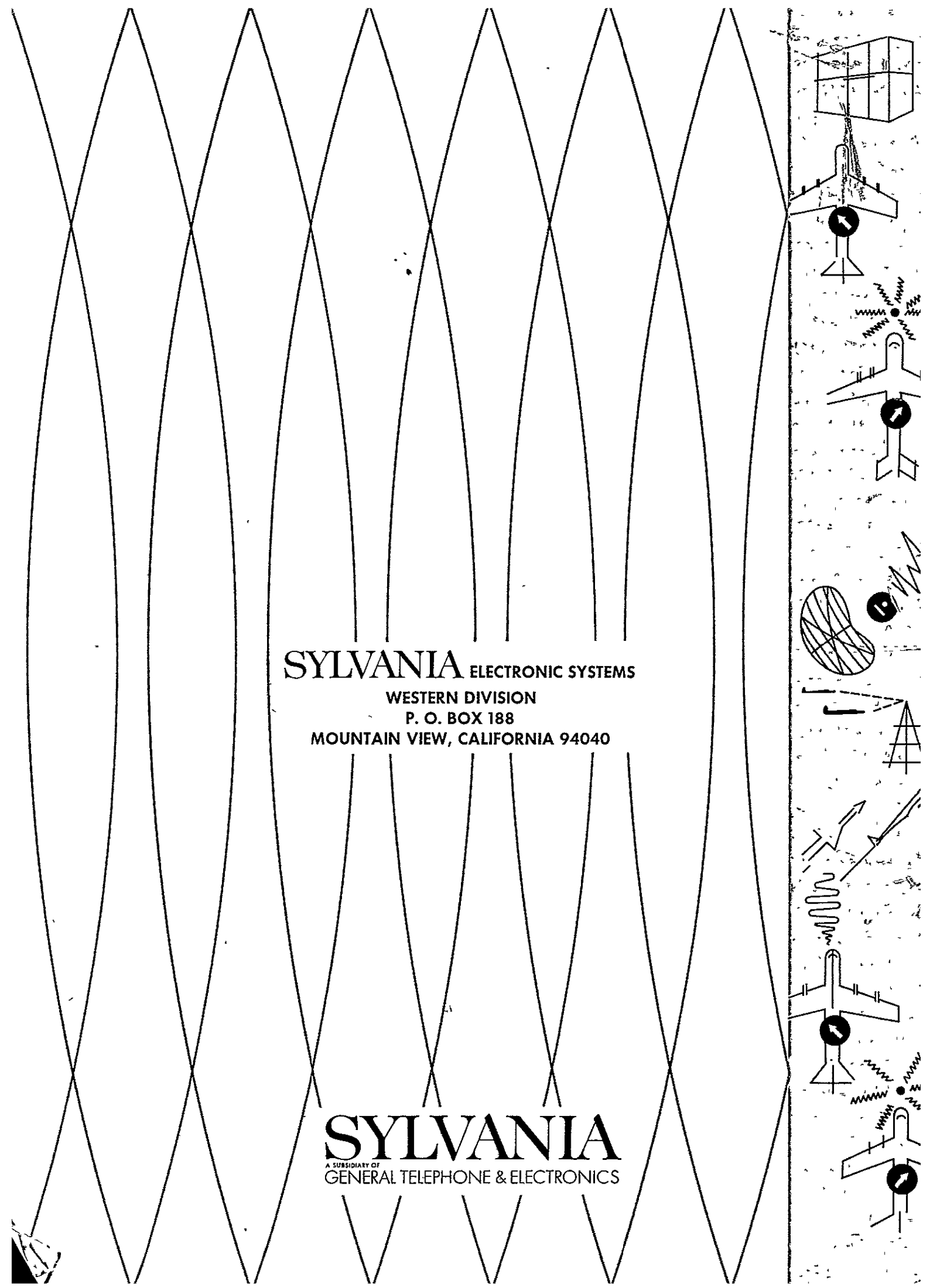

SYLVANIA ELECTRONIC SYSTEMS
WESTERN DIVISION
P. O. BOX 188
MOUNTAIN VIEW, CALIFORNIA 94040

SYLVANIA
A SUBSIDIARY OF
GENERAL TELEPHONE & ELECTRONICS